

# Assembling Atomically Precise Noble Metal Nanoclusters Using Supramolecular Interactions

Abhijit Nag and Thalappil Pradeep\*

Cite This: *ACS Nanosci. Au* 2022, 2, 160–178

Read Online

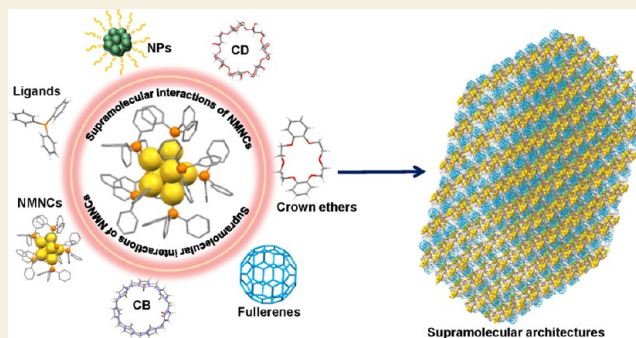
ACCESS |

Metrics &amp; More

Article Recommendations

**ABSTRACT:** Supramolecular chemistry (SC) of noble metal nanoclusters (NMNCs) is one of the fascinating areas of contemporary materials science. It is principally concerned with the noncovalent interactions between NMNCs, as well as between NMNCs and molecules or nanoparticles. This review focuses on recent advances in the supramolecular assembly of NMNCs and applications of the resulting structures. We have divided the topics into four distinct subgroups: (i) SC of NMNCs in gaseous and solution phases, (ii) supramolecular interactions of NMNCs in crystal lattices, (iii) supramolecular assemblies of NMNCs with nanoparticles and NMNCs, and (iv) SC of NMNCs with other molecules. The last explores their interactions with fullerenes, cyclodextrins, cucurbiturils, crown ethers, and more. After discussing these topics concisely, various emerging properties of the assembled systems in terms of their mechanical, optical, magnetic, charge-transfer, etc. properties and applications are presented. SC is seen to provide a crucial role to induce new physical and chemical properties in such hybrid nanomaterials. Finally, we highlight the scope for expansion and future research in the area. This review would be useful to those working on functional nanostructures in general and NMNCs in particular.

**KEYWORDS:** *supramolecular chemistry, noncovalent interactions, nanoclusters, assemblies, functional nanostructures*



## 1. INTRODUCTION

Supramolecular chemistry (SC) deals with the creation of structures and associated functions through noncovalent interactions between molecules. These reversible interactions originating from hydrophobic forces, van der Waals (vdWs) forces, hydrogen bonds, and metal–ligand binding are crucial to understand self-assembling systems and various biological processes as well as to design molecular machines. SC has developed into a prominent interdisciplinary research area including biology, chemistry, nanotechnology, materials science, and physics. It has also led to some of the important advancements in molecular science. Research in this area is advancing at an accelerated pace, and all the frontier journals present these fascinating directions. Jean-Marie Lehn, Charles J. Pedersen, and Donald J. Cram have shared the Nobel Prize in chemistry (1987) for their research on “host–guest” assemblies. In 2016, Ben Feringa, Fraser Stoddart, and Jean-Pierre Sauvage were awarded the Nobel Prize in chemistry for their work on the design and synthesis of tiny molecular machines, utilizing principles of supramolecular chemistry. It is worth noting that supramolecular assemblies could be designed to carry out specific functions. Today, such assemblies are possible with noble metal nanoclusters (NMNCs), although

many of the functions of such assemblies are yet to be explored.

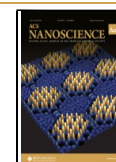
NMNCs are emerging materials due to their unique physical and chemical properties.<sup>1,2</sup> They are made of a metal core connected by staple motifs, further stabilized by a monolayer of ligands such as thiolates, phosphines,<sup>3–5</sup> carbenes,<sup>2</sup> alkynyls,<sup>6,7</sup> or a mixture of ligands.<sup>8–10</sup> Atomically precise NMNCs such as  $[\text{Au}_{25}(\text{SR})_{18}]^-$  (refs 11 and 12),  $[\text{Au}_{102}(\text{SR})_{44}]$ ,<sup>13</sup>  $[\text{Au}_{144}(\text{SR})_{60}]$ ,<sup>14,15</sup>  $[\text{Au}_{52}(\text{TBBT})_{32}]$ ,<sup>16</sup>  $[\text{Au}_{38}(\text{SR})_{24}]$ ,<sup>17</sup>  $[\text{Ag}_{29}(\text{S}_2\text{R})_{12}]^{3-}$  (ref 18),  $[\text{Ag}_{25}(\text{SR})_{18}]^-$  (ref 19),  $[\text{Ag}_{44}(\text{SR})_{30}]^{4-}$  (ref 20), and  $[\text{PdAu}_{24}(\text{SR})_{18}]^{21}$  (SR– a thiolate ligand) have precise molecular formulas, could be charged or uncharged, and exhibit unusual molecular properties. Examples include well-defined optical absorption and emission due to quantized energy levels, electrochemical properties, chirality, and chemical reactivity.<sup>1,2,22–27</sup> Limited investigations have been performed on their collective

Received: October 25, 2021

Revised: December 20, 2021

Accepted: December 21, 2021

Published: January 10, 2022



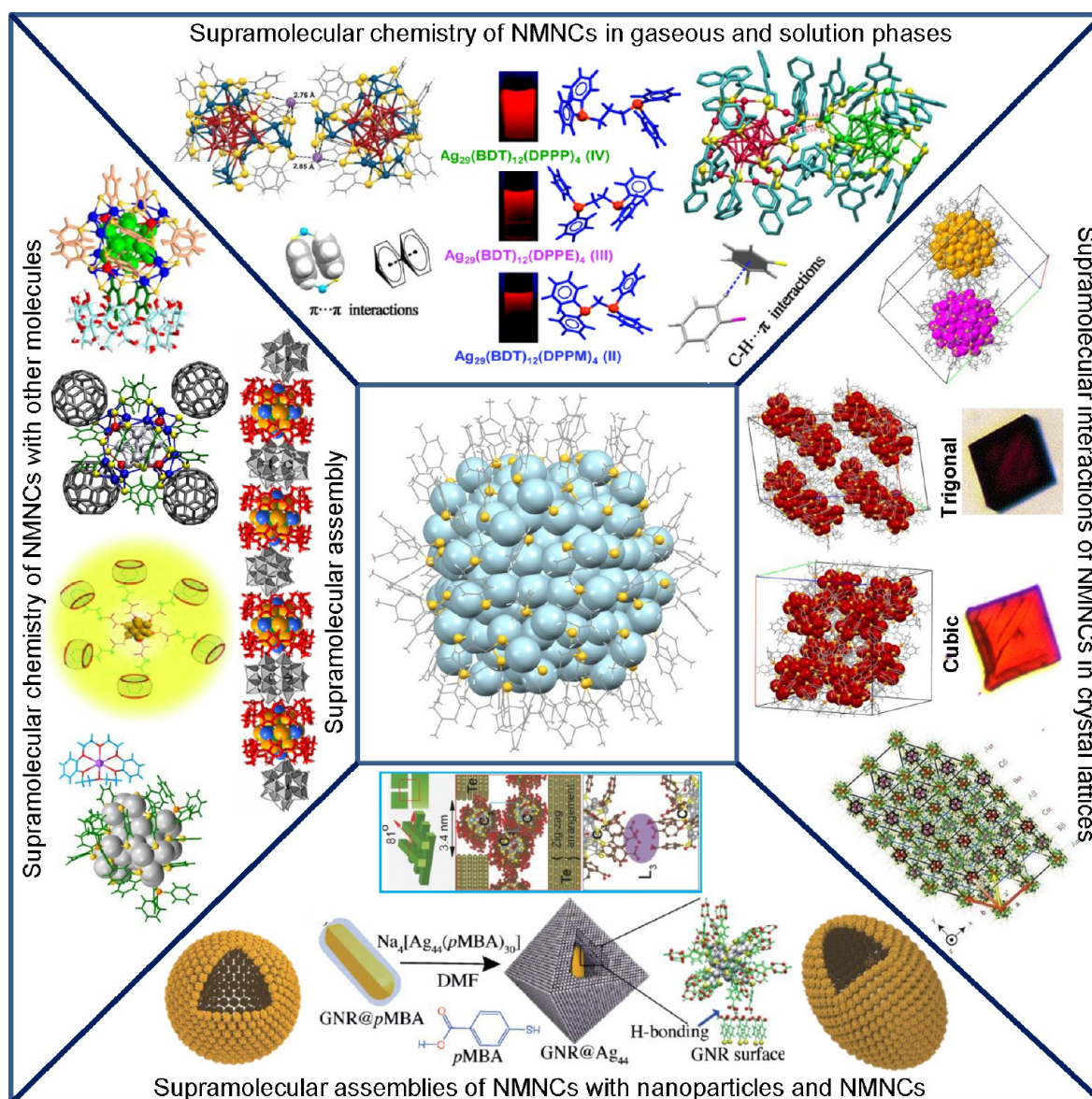


**Figure 1.** Various kinds of supramolecular assemblies of atomically precise NCs. Individual structures have been gathered from refs 20, 38, 43, 44, 46, 48, 53, 64, 65, 67, 69, 81, 82, 86, and 101. At the center, an isolated ligand-protected cluster has been redrawn from ref 47.

properties such as magnetism. The presence of various kinds of ligands on the metal core enables the possibility of making specific noncovalent interactions with NMNCs, nanoparticles (NPs), and other molecules.<sup>28–31</sup> There are also possibilities of forming inclusion complexes of ligands acting as guests with suitable hosts for the SC of NMNCs. Examples of this branch of NMNCs-assembled materials are beginning to be available. As a result, the rich diversity in this category of materials is definite to make a lasting impact on materials science. In this context, we wish to present a review of the area reflecting on the past and present potential directions for the future.

Here, we focus on various possibilities of supramolecular assemblies of NMNCs and categorize them into the following specific topics (Figure 1):

1. SC of NMNCs in gaseous and solution phases
2. Supramolecular interactions of NMNCs in crystal lattices
3. Supramolecular assemblies of NMNCs with nanoparticles and NMNCs

#### 4. SC of NMNCs with other molecules

In gaseous and solution phases, physical interactions such as vdWs,  $\pi\cdots\pi$ ,  $\pi\cdots\text{H}-\text{C}$ , electrostatic, etc. can be present. But in the crystalline state, combinations of these interactions exist. SC of NMNCs is largely arising from interactions of the ligands, and the energy involved in them is 1–2 orders lower than in typical covalent bonds. Therefore, the resulting structures will follow the general trends of supramolecular interactions of organic molecules in gaseous, solution, and crystalline states. Additional properties could arise in the case of NMNCs when a highly ordered self-assembly is formed using SC. Such examples are also discussed below. While there are several sources of excitement, there are many challenges too; we will point to a few of them in the last section of the review. A key point to bear in mind is that the structures of most of the NMNCs lattices are not completely resolved with counterions and solvents to understand all the supramolecular interactions in detail as in organic crystals.

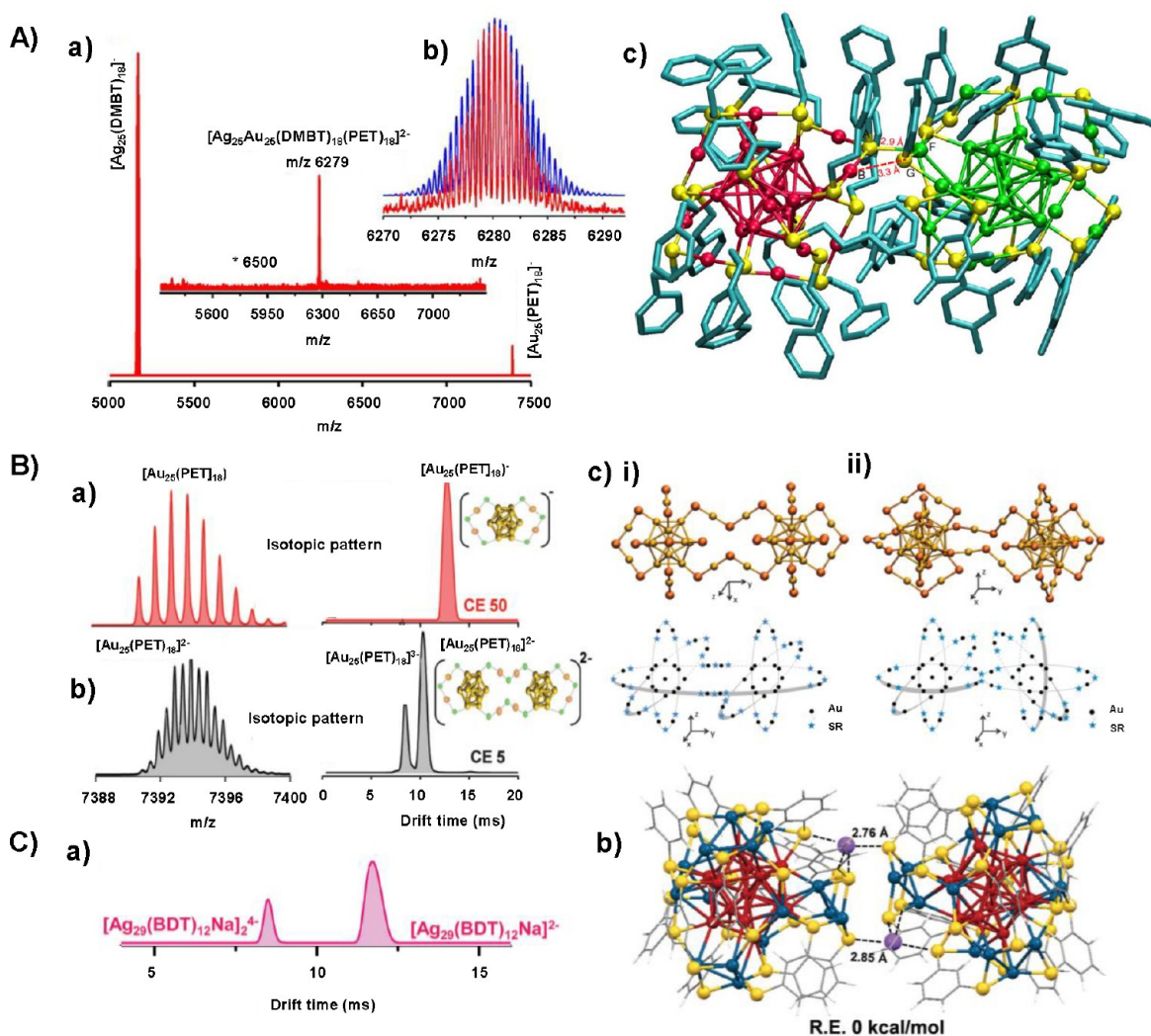


**Figure 2.** (A) (a) Formation of  $[\text{Au}_{25}\text{Ag}_{25}(\text{PET})_{18}(\text{DMBT})_{18}]^{2-}$  heterodimer via intercluster reaction between  $[\text{Ag}_{25}(\text{DMBT})_{18}]^{1-}$  and  $[\text{Au}_{25}(\text{PET})_{18}]^{1-}$ . (b) Experimental and calculated isotopic patterns for the dimer confirming the charge state of  $2^-$ . (c) DFT optimized structure of the adduct  $[\text{Au}_{25}\text{Ag}_{25}(\text{PET})_{18}(\text{DMBT})_{18}]^{2-}$ . Color codes: white, H; yellow, S; red, Au; green, Ag; cyan, C. (Reproduced from ref 38. Copyright 2016 Nature Publishing Group.) (B) (a and b) Isotopic patterns and mobility distributions of  $[\text{Au}_{25}(\text{PET})_{18}]^{1-}$  and  $[\text{Au}_{50}(\text{PET})_{36}]^{2-}$  at the collision energies (CEs) 30 and 5 eV, respectively. With the increase of CE, the dimer is converted to a monomer. (c) DFT optimized structure and Borromean ring model of  $[\text{Au}_{50}(\text{PET})_{36}]^{2-}$ . Color codes: pale red, S; orange, Au. (Adopted from ref 39. Copyright 2016 Royal Society of Chemistry.) (C) (a) Mobility distributions of  $[\text{Ag}_{29}(\text{S}_2\text{R})_{12}\text{Na}]_2^{4-}$  and  $[\text{Ag}_{29}(\text{S}_2\text{R})_{12}\text{Na}]_2^{2-}$  with different drifts ( $\text{S}_2\text{R} = \text{BDT}$ : 1,3-benzenedithiol). (b) DFT optimized structure of  $[\text{Ag}_{29}(\text{S}_2\text{R})_{12}\text{Na}]_2^{4-}$ . Color codes: yellow, S; blue and red, Ag; purple, Na; white, H; gray, carbon. (Adopted from ref 43. Copyright 2016 Royal Society of Chemistry.)

## 2. SC OF NMNCs IN GASEOUS AND SOLUTION PHASES

SC of NMNCs in gaseous and solution phases was studied mainly using mass spectrometry (MS). In this context, intercluster reactions, dimerization of NMNCs, and ligand–NMNCs interactions are discussed below. We note that intercluster reaction and dimerization of NMNCs are the outcomes of supramolecular interactions.

### 2.1. Intercluster Chemistry of NMNCs

Alloying of NMNCs can be achieved easily via intercluster reactions.<sup>32–36</sup> Reaction between two well-known NMNCs,  $[\text{Ag}_{44}(\text{SR}_1)_{30}]^{4-}$  and  $[\text{Au}_{25}(\text{SR})_{18}]^{-}$  (where  $\text{SR}_1$  and  $\text{SR}_2$  were 4-fluorothiophenol and 2-phenylethanethiol, respectively), led to the alloy NMNCs  $[\text{Ag}_x\text{Au}_{44-y}(\text{SR}_1)_{30-n}(\text{SR}_2)_n]$  and  $[\text{Au}_x\text{Ag}_{25-x}(\text{SR}_2)_{18-m}(\text{SR}_1)_m]$ .<sup>37</sup> Another example is the intercluster reaction between  $[\text{Ag}_{25}(\text{DMBT})_{18}]^{-}$  and

$[\text{Au}_{25}(\text{PET})_{18}]^{-}$ , and alloying of NMNCs occurred keeping their  $[\text{M}_{25}(\text{SR})_{18}]^{-}$  structure and topology intact, via the dianionic adduct,  $[\text{Au}_{25}\text{Ag}_{25}(\text{PET})_{18}(\text{DMBT})_{18}]^{2-}$  (Figure 2Aa and b).<sup>38</sup> All these studies were principally based on MS. Density functional theory (DFT) calculation and molecular docking studies suggested that  $\pi\cdots\pi$ ,  $\pi\cdots\text{H}-\text{C}$ , and metal-philic interactions were the main reasons for such intercluster reactions to be initiated (Figure 2Ac). It may seem that there could be a repulsive force between the two anionic NMNCs when they approach each other. However, the overall charges of these NMNCs,  $[\text{Ag}_{25}(\text{SR})_{18}]^{-}$  and  $[\text{Au}_{25}(\text{SR})_{18}]^{-}$ , are not confined but distributed over all the atoms in their staples, core, and ligands. As a result, the two NMNCs do not feel reasonable repulsive interactions between them. vdWs interactions between the NMNCs are playing a key role for such intercluster reactions as the atom exchange gets initiated

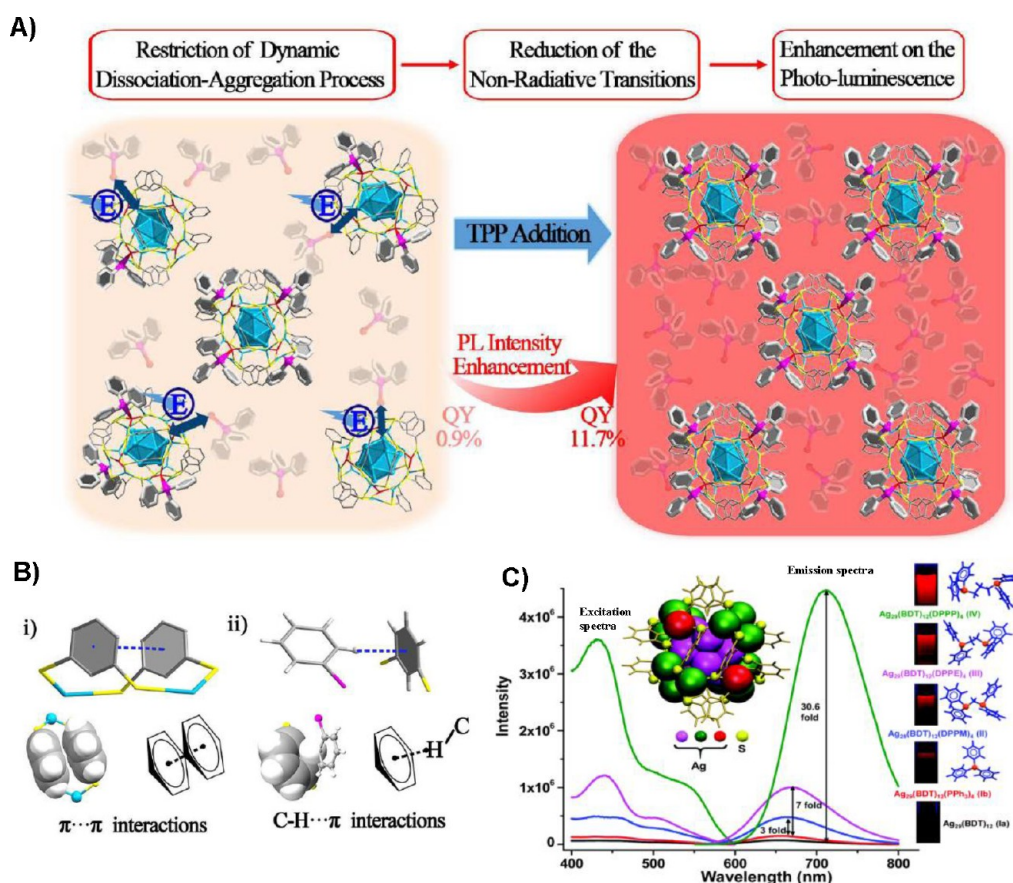


**Figure 3.** (A) Schematic representation of the luminescent enhancement of  $[\text{Ag}_{29}(\text{S}_2\text{R})_{12}(\text{TPP})_4]$  in solution by the dissociation–aggregation process ( $\text{S}_2\text{R} = \text{BDT}$ ). (B) (i)  $\pi\cdots\pi$  interaction between  $\text{S}_2\text{R}$  ligands and (ii)  $\pi\cdots\text{H}-\text{C}$  interaction between  $\text{S}_2\text{R}$  and TPP ligands, respectively. (Reproduced from ref 44. Copyright 2018 Royal Society of Chemistry.) (C) Emission and excitation spectra of NCs with different secondary ligands; each set is presented using the same color code. The DFT optimized structure of  $[\text{Ag}_{29}(\text{S}_2\text{R})_{12}]$  is presented in the inset. About 30 times enhancement in PL intensity related to its parent NMNC,  $[\text{Ag}_{29}(\text{S}_2\text{R})_{12}(\text{TPP})_4]$ , was confirmed when TPP was replaced with DPPP. (Reproduced from ref 46. Copyright 2018 Royal Society of Chemistry.)

by the formation of intercluster adducts,<sup>34,35</sup> which have been detected by MS (Figure 2A).

## 2.2. Dimerization of NMNCs

Dimerization and aggregation of NMNCs occurred due to the presence of noncovalent interactions. Our group reported the aggregation of  $[\text{Au}_{25}(\text{SR})_{18}]^-$  in the gas phase using ion mobility (IM) MS.<sup>39</sup> The trimer, dimer, and monomer of  $[\text{Au}_{25}(\text{SR})_{18}]^-$  were separated because of their difference in collision cross sections. As a result, different drift times were observed for them in the mobility distribution. The isotopic patterns and mobility distributions of  $[\text{Au}_{25}(\text{PET})_{18}]^{1-}$  and  $[\text{Au}_{50}(\text{PET})_{36}]^{2-}$  at the collision energies (CEs) 30 and 5 eV are presented in Figure 2Ba and b, respectively. DFT calculations revealed that noncovalent and aurophilic interactions are the primary causes for the gas-phase aggregation of  $[\text{Au}_{25}(\text{SR})_{18}]^-$  (Figure 2Bc). However, despite having a similar structure,  $[\text{Ag}_{25}(\text{SR})_{18}]^-$  did not produce such a dimer in the gas phase. Bidentate thiol ligand can play a crucial role to assemble thiolated NMNCs into multimers. Recently, Bodiuzzaman et al. reported a covalently linked dimer of  $[\text{Ag}_{25}(\text{SR})_{18}]^-$  which was also confirmed using MS and supported by DFT calculations and other techniques.<sup>40</sup> Dimers of  $[\text{Au}_{25}(\text{S}-t\text{Bu})_{18}]^-$  were obtained using bidentate benzene-1,4-dithiol as a ligand.<sup>41</sup> Similarly, Lahtinen et al. confirmed the formation of a dimer of  $[\text{Au}_{102}(\text{SR})_{44}]$  and  $[\text{Au}_{250}(\text{SR})_n]$

using transmission electron microscopy (TEM) where biphenyldithiols (BPDTs) were used as a linker.<sup>42</sup>

In another report, dimerization of  $[\text{Ag}_{29}(\text{S}_2\text{R})_{12}]^{3-}$  induced by alkali metal ions was investigated using IM MS in the gas phase.<sup>43</sup> The proton affinity of the same metal cluster was also studied. Dimers induced by  $\text{H}^+$  and  $\text{Li}^+$  were not detected because these cations are smaller in size.  $\text{Na}^+$ ,  $\text{K}^+$ ,  $\text{Rb}^+$ , and  $\text{Cs}^+$  induced dimer formations were studied using IM MS. The mobility distributions of  $[\text{Ag}_{29}(\text{S}_2\text{R})_{12}\text{Na}]^{2-}$  and  $[\text{Ag}_{29}(\text{S}_2\text{R})_{12}\text{Na}]^{4-}$  with different drift times are shown in Figure 2Ca. The dimerization process was assisted by the interactions between the sulfur of the NMNCs and the cations (Figure 2Cb).

## 2.3. Interactions of NMNCs with Ligands

Ligand–ligand and NMNC–ligand interactions play a crucial role to build the SC of NMNCs in gaseous and solution phases. In this context, Zhu and co-workers reported a novel mechanism of aggregation induced emission where the restriction of the “dissociation–aggregation pattern” of ligands is explained using  $[\text{Ag}_{29}(\text{S}_2\text{R})_{12}(\text{TPP})_4]$  (TPP: triphenylphosphine) (termed as  $\text{Ag}_{29}$ ) as an example (Figure 3A).<sup>44</sup> To prove the dissociation–aggregation process, different concentrations of TPP molecules were added to the nondissociative  $[\text{Ag}_{28}\text{Pt}_1(\text{Adm})_{18}(\text{TPP})_4]$ <sup>45</sup> (termed as  $\text{Ag}_{28}\text{Pt}_1$ ) (Adm: 1-adamantanethiol) and dissociative  $\text{Ag}_{29}$  solution. The photo-

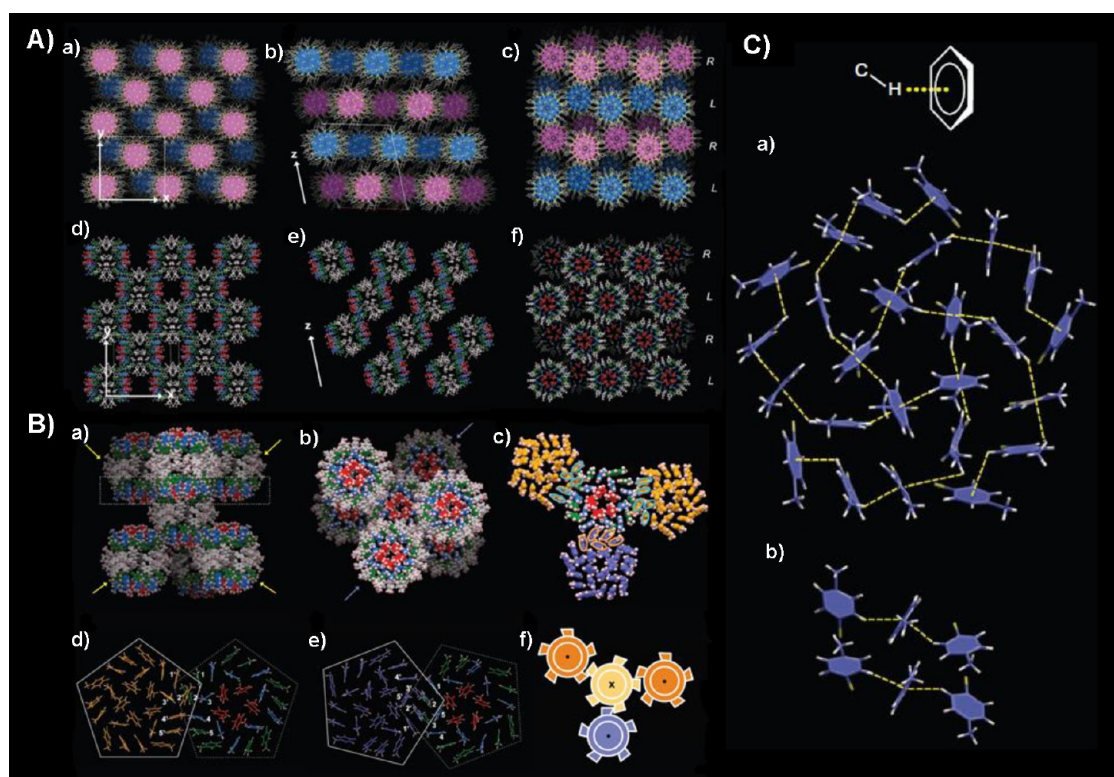


**Figure 4.** (A) Packing of  $[\text{Au}_{246}(\text{p-MBT})_{80}]$  in the unit cell. Views from the (a)  $z$ -direction, (b)  $y$ -direction, (c) and  $x$ -direction. Color codes:  $[\text{Au}_{246}(\text{p-MBT})_{80}]$  with different chirality, gold, blue, and magenta; sulfur, yellow; carbon, gray. (d–f) Arrangement of ligands of  $[\text{Au}_{246}(\text{p-MBT})_{80}]$  along the  $z$ -,  $y$ -, and  $x$ -directions. Color codes: ligands positioned at the middle of  $[\text{Au}_{246}(\text{p-MBT})_{80}]$ , gray, red, blue, and green; ligands positioned at the extremes, green, blue, and red. (B) Intercluster self-assembly generated by the ligands. (a and b) Coordination geometry of  $[\text{Au}_{246}(\text{p-MBT})_{80}]$  in the unit cell: side view (a) and top view (b). (c) Interactions among the intercluster ligands. (d) Side-by-side assembly of the ligands in  $[\text{Au}_{246}(\text{p-MBT})_{80}]$  with the same chirality. (e) Point-to-point assembling of the ligands in  $[\text{Au}_{246}(\text{p-MBT})_{80}]$  with opposite chirality. (f) Schematic representation of the directional packing of  $[\text{Au}_{246}(\text{p-MBT})_{80}]$ . (C) Various  $\pi \cdots \text{H}-\text{C}$  interactions between the ligands of NMNC: (a) rotational and (b) parallel patterns. (Reproduced from ref 47. Copyright 2016 American Association for the Advancement of Science.)

luminescence (PL) intensity of  $\text{Ag}_{29}$  was improved 13 times by the addition of TPP into  $N,N$  dimethylformamide (DMF) solution of the NMNC. But the PL intensity of nondissociative  $\text{Ag}_{28}\text{Pt}_1$  remained almost the same after the addition of TPP. A temperature-dependent PL study of  $\text{Ag}_{29}$  NC showed two stages of intensity increase.<sup>44</sup> This confirmed that both the quenched thermal vibration process and the restriction of the TPP dissociation–aggregation process were involved in  $\text{Ag}_{29}$ . However, only the thermal vibration process was observed for  $\text{Ag}_{28}\text{Pt}_1$ . The  $\pi \cdots \pi$  and  $\pi \cdots \text{H}-\text{C}$  interactions between the ligands are shown in Figure 3B.

In a subsequent study, Khatun et al. demonstrated that systematic replacement of the TPP with other secondary ligands resulted in an enhancement of PL intensity of  $\text{Ag}_{29}$  in the NIR (near-infrared) region.<sup>46</sup> Secondary ligands also play a vital role to enhance the photoluminescence of NMNCs. About 30 times enhancement in PL intensity related to the parent NMNC,  $[\text{Ag}_{29}(\text{S}_2\text{R})_{12}(\text{TPP})_4]$ , was confirmed when TPP was replaced with 1,3-bis(diphenylphosphino)propane (DPPP) (Figure 3C). DFT calculations of the NMNC with different secondary ligands suggested that the emission was due to a LMCT (ligand to metal charge transfer). Enhancement of the luminescence was because of restricted intramolecular rotation (RIR). The rigidity of the NMNC surface was increased when TPP was replaced with DPPP because of the presence of a greater number of noncovalent interactions ( $\pi \cdots \pi$  and  $\pi \cdots \text{H}-\text{C}$  interactions) in DPPP capped NMNCs.

The rigidity of the NC promoted the radiative transitions by allowing RIR. A similar type of result was also observed for  $[\text{Ag}_{51}(\text{S}_2\text{R})_{19}(\text{TPP})_3]$ .<sup>46</sup>

### 3. SUPRAMOLECULAR ASSEMBLIES OF NMNCs IN CRYSTAL LATTICES

Supramolecular interactions could play an important role in the systematic organization of NMNCs in crystal lattices. Well-organized assembly of NMNCs is present in their unit cells. An understanding of the packing arrangement of NMNCs in a crystal lattice could provide new insights into the NMNC-assembled patterns, structures, and properties. In this section, supramolecular interactions of NMNCs via intercluster and intracluster fashions in crystal lattices are presented.

#### 3.1. Ligand Induced Supramolecular Assemblies of NMNCs in Crystal Lattices

Supramolecular interactions among ligands present in a crystal lattice generate various unique patterns, structures, and properties. In this section, we will focus on various supramolecular interactions among ligands leading to different symmetries and patterns.

For example, Jin and co-workers determined the structure of  $[\text{Au}_{246}(\text{p-MBT})_{80}]$  ( $\text{p-MBT} = p$ -methylbenzenethiolate) at the atomic, molecular, and nanoscale levels using SCXRD (single crystal X-ray diffraction).<sup>47</sup> The ligands generated complex patterns on the NMNC surfaces similar to structures of biomolecules. The density and symmetry of the surface

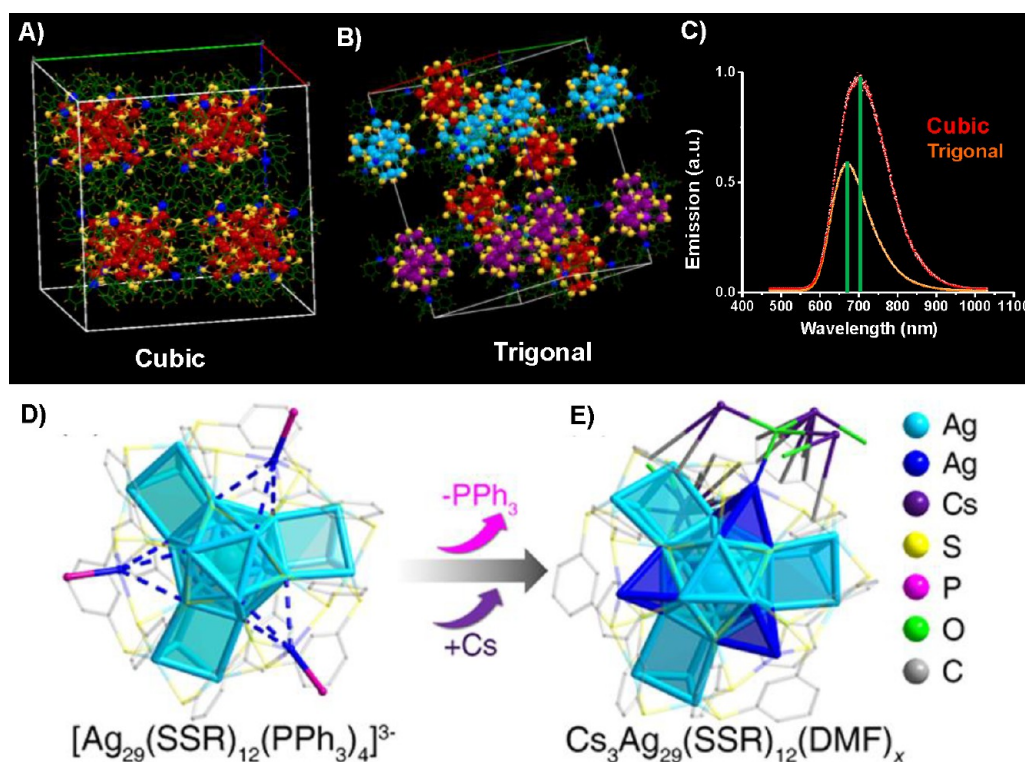


**Figure 5.** (A) Cubic unit cell and (B) trigonal unit cell of  $Ag_{29}$  NMNC. (C) Emission spectra of the cubic and trigonal crystals of the NMNC. (Adopted from ref 53. Copyright 2018 Royal Society of Chemistry.) (D) Structure of  $Ag_{29}$  NMNC. (E) Crystal structure of  $[Ag_{29}Cs_3(S_2R)_{12}(DMF)_m]$  ( $m = 5, 6$ ). (Adopted from ref 58. Copyright 2019 American Chemical Society.)

patterns further guided the packing of NMNCs into lattices with rotational, orientational, and translational order.  $[Au_{246}(p-MBT)_{80}]$  NMNCs are presented with a square configuration in Figure 4Aa, akin to the packing mode in the [100] plane of fcc metals. The NMNCs are stacked obliquely along the [001] direction (Figure 4Ab). The packing density of the NMNCs is 60%, which is less than the fcc lattice (74%). The consequence of specific intercluster interactions of the monoclinic packing is correlated to the alignment of the ligands on the NMNCs (Figure 4Ad–f). The crystal lattice was verified to possess an ABAB type of arrangement, wherein  $[Au_{246}(p-MBT)_{80}]$  makes up the A layer and isomeric NMNCs are the B layer (i.e., (R-NC)A@(L-NC)B@(R-NC)A@(L-NC)B), shown in Figure 4Ac. To realize the intercluster assembly of  $[Au_{246}(p-MBT)_{80}]$ , the coordination environment of the surface ligands was also examined (Figure 4Ba–f). Each NMNC is surrounded by six neighboring NMNCs. Four of them have the same chirality as the central one (Figure 4Ba, yellow arrows). They are organized within the same square layer. The other two are of the opposite chirality in different layers (Figure 4Bb, purple arrows). The peripheral ligands of a NMNC interacted with other ligands from three neighboring NMNCs, and five pairs of interacted ligands contributed to each interaction (Figure 4Bc). Intermolecular  $\pi \cdots H-C$  interactions play a key role to stabilize the surface patterns on the NMNCs. The C–H bonds of the methyl groups or phenyl rings interact with the  $\pi$  electrons (Figure 4Ca and b). The ligand's rotational and parallel self-assembled surface patterns are comparable to the structural complexity of biomolecules such as the  $\alpha$ -helix and  $\beta$ -sheet in proteins.

Similarly,  $[Au_{144}(PMT)_{60}]^{48}$  (PMT = S-CH<sub>2</sub>Ph) and  $[Au_{133}(PET)_{52}]^{49}$  (SR = S-C<sub>2</sub>H<sub>4</sub>Ph) NMNCs are arranged with an ABAB packing mode (i.e., (R-NC)A@(L-NC)B@(R-

NC)A@(L-NC)B) like the above-mentioned  $[Au_{246}(p-MBT)_{80}]$ . The asymmetric arrangement of the surface structures results in isomerism in NMNCs. Intercluster interactions were observed between the two neighboring  $[Au_{144}(PMT)_{60}]$  NMNCs. The optical isomers (R and L) were stacked layer by layer with a hexagonal pattern in the (001) plane and a square configuration in the (100) and (010) planes. Each  $[Au_{144}(PMT)_{60}]$  was surrounded by six  $[Au_{144}(PMT)_{60}]$  NMNCs with the opposite chirality in the crystal lattice. Various kinds of supramolecular interactions such as  $\pi \cdots H-C$  (2.80 Å) and  $H \cdots H$  (2.54 Å) between the ligands of neighboring NMNCs lead to the formation of compact and ordered crystal structures.

The ABAB (e.g.,  $[Au_{246}(p-MBT)_{80}]$ ,  $[Au_{133}(PET)_{52}]$ , and  $[Au_{144}(PMT)_{60}]$ ) and the ABCD (e.g.,  $[Au_{92}(SR)_{44}]$ )<sup>50</sup> are the two well-known packing fashions of the NMNC system. Recently, a third mode of packing—ABCDEF (6H packing mode)—was reported for  $[Au_{60}S_6(PMT)_{36}]$  by Gan et al.<sup>51</sup> In their work, Gan et al. incorporated a sulfur atom on  $[Au_{60}S_6(PMT)_{36}]$  and converted it into  $[Au_{60}S_7(PMT)_{36}]$  by heating. As a consequence, the ABCDEF (6H packing mode) arrangement in  $[Au_{60}S_6(PMT)_{36}]$  was converted into the ABAB mode for  $[Au_{60}S_7(PMT)_{36}]$ , although the crystallization conditions were identical. The difference in the packing in the unit cell was reflected in the optical properties. The PL intensity of the  $[Au_{60}S_6(PMT)_{36}]$  (ABCDEF-6H packing mode) crystal lattices is weaker compared to  $[Au_{60}S_7(PMT)_{36}]$  (ABAB packing mode) in the amorphous state.  $[Ag_{46}S_7(SR)_{24}]$  (SR = S-PhMe<sub>2</sub>) packed with the ACB@ACB mode (simple translational symmetry) in the crystal lattice.<sup>52</sup> Each NMNC is connected with four other NMNCs in other planes. C–H $\cdots\pi$  interactions (intracluster) between adjacent ligands resulted in

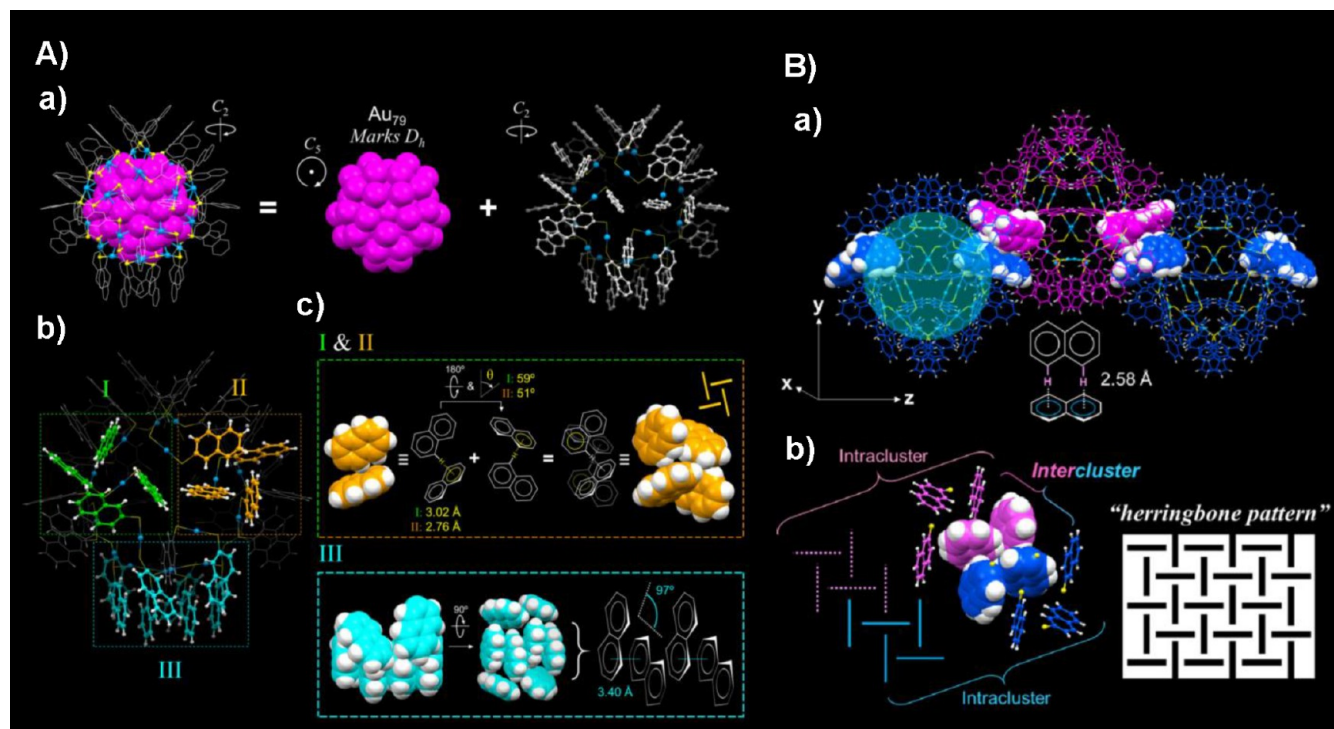


**Figure 6.** (A) (a) Crystal structures of the  $[\text{Au}_{103}\text{S}_2(\text{S-Nap})_{41}]$  NMNC,  $\text{Au}_{79}$  (middle), and ligands (right). Color codes: magenta and blue, Au; yellow, S; white, H. (b) Intracuster interactions via ligands. (c) T-shaped arrangement adopted a “herringbone pattern” via  $\pi\cdots\text{H}-\text{C}$ . (B) (a) Intercluster interactions ( $\pi\cdots\text{H}-\text{C}$ ) in the crystal lattice of  $\text{Au}_{103}$  NMNC. (b) Intercluster and intracuster interactions resulted in the “herringbone pattern”. (Adopted from ref 54. Copyright 2017 American Chemical Society.)

the systematic organization of the ligands on the NMNC surface.

Supramolecular interactions can be tuned to generate a polymorphic NMNC crystal lattice.<sup>53</sup> In this context, a cubic lattice (C) of  $[\text{Ag}_{29}(\text{S}_2\text{R})_{12}(\text{TPP})_4]$  was obtained using the drop-casting method (Figure 5A).  $[\text{Ag}_{29}(\text{S}_2\text{R})_{12}(\text{TPP})_4]$  adopted the trigonal lattice (T) when the vapor diffusion method was used (Figure 5B). The T unit cell was composed of three different orientations of the NMNCs (highlighted in different colors), whereas only one type of orientation of the NMNCs was confirmed in the C unit cell (Figure 5A and B). The difference in the intercluster interactions of TPP and S<sub>2</sub>R resulted in two polymorphic crystals. The  $\pi\cdots\text{H}-\text{C}$  interactions of TPP were more favored in a C lattice compared to a T lattice. The greater numbers of  $\pi\cdots\text{H}-\text{C}$  interactions resulted in a greater rigidity in the C system relative to the T system. This is why the cubic crystals gave rise to a greater PL intensity compared to trigonal crystals (Figure 5C).

In another study, the SCXRD of  $[\text{Au}_{103}\text{S}_2(\text{NPT})_{41}]$  (NPT = 2-naphthalenethiol) revealed the “intercluster assembly” of NMNCs (Figure 6Aa).<sup>54</sup> The surfaces of the NMNCs are highly stabilized through intracuster noncovalent interactions, such as  $\text{H}\cdots\text{H}$  and  $\pi\cdots\text{H}-\text{C}$  interactions. Intercluster and ligand–ligand interactions resulted in highly dense assembly in the unit cell (Figure 6Ab). Naphthalene thiols on the NMNC surface created local tetramers through noncovalent interactions of  $\pi\cdots\pi$  and  $\pi\cdots\text{H}-\text{C}$  stacking (Figure 6Ac). The outer surfaces of the ligands of neighboring NMNCs are interlinked via T-shaped  $\text{C}-\text{H}\cdots\pi$  interactions with an average distance of 2.58 Å to yield intercluster assembly (Figure 6Ba). Such an orderly T-shaped arrangement adopted a “herringbone pattern” via intercluster interactions (Figure 6Bb). These

types of patterns have resulted in a linearly connected zigzag arrangement in the unit cell.

Recently, Khatun et al. reported an assembly of NMNCs coprotected by diphosphine and thiol,  $[\text{Ag}_{22}(\text{SR})_{12}(\text{DPPE})_4\text{Cl}_4]^{2+}$  (SR = 2,5-dimethylbenzenethiol; DPPE = 1,2-bis(diphenylphosphino)ethane).<sup>55</sup> The NMNC consisted of an  $\text{Ag}_{10}$  core and  $[\text{Ag}_{12}(\text{DPPE})_4(2,5\text{-DMBT})_{12}\text{Cl}_4]$  shell. The  $[\text{Ag}_{12}(\text{SR})_{12}(\text{DPPE})_4\text{Cl}_4]$  shell encapsulated the  $\text{Ag}_{10}$  core. Electrospray ionization (ESI) MS study also supported the SCXRD data. An unusual crystallization induced luminescence enhancement was confirmed for this NMNC as the emission was weak in the amorphous states and solution. However, about 12 times luminescent enhancement was observed in the case of the crystalline state relative to the amorphous state. As the NMNC is protected by DPPE and DMBT, the well-organized noncovalent interactions ( $\pi\cdots\text{H}-\text{C}$  and  $\pi\cdots\pi$ ) between the ligands throughout the crystal lattice led to the enhancement in luminescence.

Negishi and co-workers reported some essential factors for the assembly of NMNCs and the functions and properties of such assembled structures.<sup>56</sup>  $[\text{Au}_4\text{Pt}_2(\text{SR})_8]^0$  was used for the study, and the following four points were mentioned about the NMNCs: (1)  $[\text{Au}_4\text{Pt}_2(\text{SR})_8]^0$  could be utilized as a building block to generate one-dimensional connected structures (1D-CS) via intercluster gold–gold bonds (aurophilic bond). (2) The intra-NC ligand interactions differed subject to the ligand structure having a similar structure of  $[\text{Au}_4\text{Pt}_2(\text{SR})_8]^0$ . Consequently, the distribution of the ligands varied depending on the structure of the ligand in  $[\text{Au}_4\text{Pt}_2(\text{SR})_8]^0$ . (3) The inter-NC ligand interactions were influenced by the changes in the distributions of the ligands. (4) The band gap of the NMNCs was reduced by the formation of 1D-CS. This study established

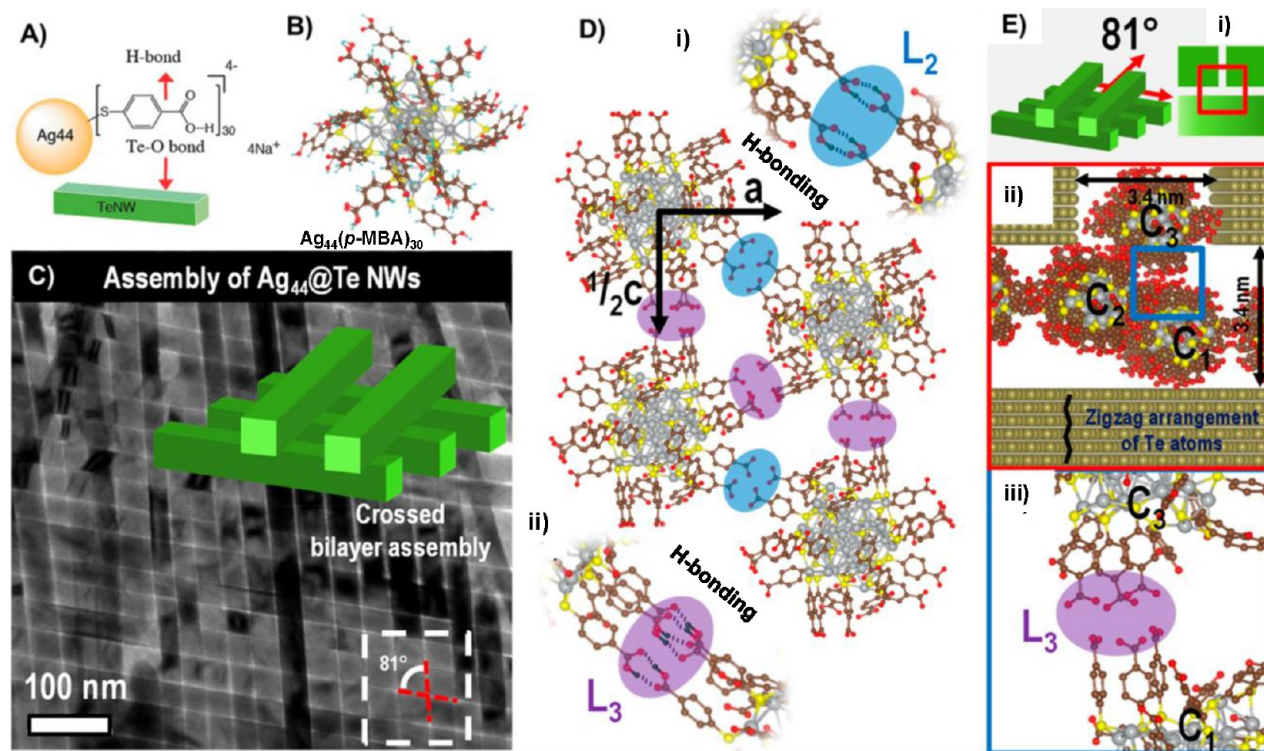


**Figure 7.** (A) Schematic representation of the interactions between  $[Ag_{44}(SR)_{30}]$  and Te NWs. (B) Total structure of  $[Ag_{44}(p\text{-MBA})_{30}]$ . (C) Formation of the crossed-bilayer assembly (CBA) of  $Ag_{44}@Te$  NWs shown via TEM images. (D) H-bonding between the carboxylic group of the ligand of adjoining. The adjoining NCs' network via H-bonding with  $L_2$  (i) and  $L_3$  (ii) fashion. (E) (i) Schematic representation of the CBA. (ii) Zoom in view of the area shown in (i). Further zoom in view is presented in (iii). Different NCs are labeled as  $C_1$ ,  $C_2$ , and  $C_3$ . (Reproduced from refs 28, 64, and 68. Copyright 2019 American Chemical Society, 2016 and 2017 Wiley.)

that intracluster ligand interactions need to be created to yield 1D-CS with desired functionalities.

Supramolecular interactions were also reported for heterocyclic carbene-protected Au superatom NMNCs  $[Au_{13}(NHC^{Bn})_9Cl_3]^{2+}$  (NHCs N-heterocyclic carbenes).<sup>57</sup> The NMNC was synthesized by the reduction of precise  $Cl-Au-NHC$  complexes. The NMNC consisted of an icosahedral  $Au_{13}$  core protected by nine NHCs and three chlorides in an ordered fashion. SCXRD revealed that the NMNCs were assembled via multiple noncovalent interactions ( $\pi \cdots H-C$  and  $\pi \cdots \pi$ ) which made the surfaces of the ligands rigid. As a result, a high quantum yield (QY) up to 16.0% was observed. The QY is considerably higher than other reported  $Au_{13}$  superatom NMNCs.

Hydrogen bonding interactions among ligands were also studied. The complete structure of  $[Ag_{44}(SR)_{30}]$  ( $SR = p$ -mercaptobenzoic acid) was resolved using X-ray crystallography.<sup>20</sup> The crystal lattice consisted of two kinds of  $Ag_{44}$  NMNCs ( $\alpha$  and  $\beta$ ) stacked in a fcc lattice. They are correlated by a mirror reflection symmetry. The ACB layers were arranged in order in a six-layer sequence— $A\alpha-C\beta-B\alpha-A\beta-C\alpha-B\beta$ —due to the presence of  $\alpha-\beta$  mirror symmetry.  $[Ag_{44}(SR)_{30}]$  produced a self-assembled structure throughout the crystal lattice through the establishment of strong H-bonds between the carboxyl groups of neighboring NMNCs. The ligands were interconnected via double and triple bundles. Intralayer H-bonding between neighboring NMNCs ( $\alpha\alpha$  or  $\beta\beta$ ) resulted in a doubly bundled ligand arrangement, whereas the interlayer H-bonding between neighboring NMNCs ( $\alpha\beta$ ) gave rise to the triply bundled ligand arrangements.<sup>21</sup>

### 3.2. Ion Induced Supramolecular Assemblies of NMNCs in Crystal Lattices

Ion induced supramolecular interactions such as electrostatic, cation $\cdots\pi$ , and anion $\cdots\pi$  interactions take crucial part in nature, particularly in molecular recognition, protein structure, and enzyme catalysis. Similarly, ions could also play an important role to assemble NMNCs via ion induced supramolecular interactions. Pradeep and co-workers reported the gas-phase adducts of  $[Ag_{29}(S_2R)_{12}]$  with alkali metals as discussed above.<sup>43</sup> Recently, Zhu and his co-workers resolved the structure of  $Cs^+$  attachment with  $[Ag_{29}(S_2R)_{12}(TPP)_4]$  using X-ray crystallography and studied the supramolecular assembly of the NMNCs.<sup>58</sup> The addition of  $Cs^+$  peeled the TPP off from the NMNC surface and resulted in a neutral  $Cs$ -NMNC complex,  $[Ag_{29}Cs_3(S_2R)_{12}(DMF)_m]$  ( $m = 5, 6$ ) (Figure 5D and E). The formation of such a complex was driven by the electrostatic attraction between  $[Ag_{29}(S_2R)_{12}(TPP)_4]^{3-}$  and  $Cs^+$  and was facilitated by  $Cs \cdots \pi$  and  $Cs-S$  interactions. The capture of  $Cs^+$  induced changes on the  $[Ag_{29}(S_2R)_{12}]$  unit. Interactions among  $[Ag_{29}(S_2R)_{12}(TPP)_4]^{3-}$ ,  $Cs^+$ , and DMF gave rise to a 1D self-assembled structure in the crystal lattice. The optical properties of  $[Ag_{29}Cs_3(S_2R)_{12}(DMF)_m]$  were changed remarkably compared to the parent NC due to such types of intercluster interactions. Similarly, hydrophobic NMNCs  $[Ag_{29}(S_2R)_{12}(PPh_3)_4]^{3-}$  were made water-soluble using solvent-conjoined  $Na^+$  by the same group.<sup>59</sup>

In a subsequent study, Hyeon and co-workers reported a simple synthesis of an assembly of highly fluorescent AuNCs. In particular,  $Zn^{2+}$  induced precise assembly of  $Au_4$  NCs exhibited a QY of  $\sim 90\%$  in water.<sup>60</sup> This is the highest QY reported for NMNCs until date.  $Zn^{2+}$  induced distinctive



aurophilic interaction (gold(I)–gold(I),  $d^{10}-d^{10}$ ) among Au<sub>4</sub> NCs, resulting in such a highly greenish-blue fluorescence. This bright fluorescence came from the Zn<sup>2+</sup> induced rigidified environment due to the delay in vibrational relaxation. This NMNC assembly may be used for the drug delivery by monitoring the reassembly and disassembly processes reversibly, by the readdition and extraction of metal ions.

Counter ions also assist in the packing arrangement of NMNC in a unit cell. The Jin group reported the variation in packing for Au<sub>23</sub>, Au<sub>21</sub>@Cl, and Au<sub>21</sub>@AgCl<sub>2</sub> NMNCs because of their differences in surface structures and counterions.<sup>61</sup> X-ray diffraction studies revealed the hierarchical assembly in the crystal lattice. Au<sub>21</sub> NCs were systematically organized into one-dimensional (1D) nanofibrils via various noncovalent interactions ( $\pi\cdots\text{anion}$ ,  $\pi\cdots\pi$ , and aryl Cl $\cdots$ H–C interactions) facilitated by site-specific surface hooks. Further, these 1D nanofibrils resulted in 3D crystals which gave rise to the hierarchical assembly. Modification of the packing arrangements of Au<sub>21</sub> NCs by modifying the counterions influenced the electrical transport properties by 2 orders of magnitude.

#### 4. SUPRAMOLECULAR ASSEMBLIES OF NMNCs WITH NANOPARTICLES AND NMNCs

Supramolecular interactions of NMNCs with NPs and NMNCs could result in self-assembled superstructures. The interactions of [Ag<sub>32</sub>(SG)<sub>19</sub>]<sup>62</sup> with 1D tellurium nanowires (Te NWs) were introduced by Pradeep and co-workers.<sup>63</sup> The reaction between Ag NPs and ions with 1D Te NWs resulted in AgTe NWs. But a different reactivity toward Te NWs was evidenced for NMNCs which lead to the formation of Ag islands at different locations on the Te NWs. Inspired by this result, Som et al. further studied the interactions between Te NWs and [Ag<sub>44</sub>(*p*-MBA)<sub>30</sub>] (MBA = S-PhCOOH) (termed as Ag<sub>44</sub>) (Figure 7A and B).<sup>64</sup> After dispersing Ag<sub>44</sub>@Te NWs in 1-butanol, the sample was kept for solvent evaporation. These hybrid material Ag<sub>44</sub>@Te NWs resulted in a crossed-bilayer structure, whereas a monolayer assembly was formed when the NMNC was absent (Figure 7C). TEM data revealed that the hybrid Ag<sub>44</sub>@Te NWs formed a woven-fabric-like structure, where the NWs were arranged in parallel fashion in the same layer but, in the adjacent layer, they were organized with an unusual angle of 81° between them. The Ag<sub>44</sub> NCs were attached onto the Te NWs' surface by Te–O interactions. Computational study demonstrated that the organization of the Te NWs between two adjacent layers with an angle of 81° assisted the formation of the strongest H-bonding because of the three pairs ( $L_3$ ) of H-bonding between the neighboring Ag<sub>44</sub> NCs layered over Te NWs (Figure 7D and E). To support these data, another NC [Au<sub>102</sub>(SR)<sub>44</sub>] was also used in the study. In this case, a similar structure was noticed, but the angle between the two adjacent layers was 77°. Such a difference in angles (81° and 77°) was due to the difference in orientation of the ligands on the two NMNC surfaces.

Recently, Chakraborty et al. explored the supramolecular assembly of [Ag<sub>44</sub>(SR)<sub>30</sub>] with gold nanorods (GNRs) through H-bonding interactions.<sup>65</sup> They employed *p*-MBA ligands to functionalize Au GNRs at neutral pH. Then, the functionalized GNRs were utilized for the assembly of [Ag<sub>44</sub>(SR)<sub>30</sub>] in DMF for 20 h. H-bonds were generated between the carboxyl groups of nearby *p*-MBA ligands for both the GNRs and Ag<sub>44</sub> NCs during this process. This resulted in a multilayer shell that encapsulated the individual GNRs. As a result, the GNRs transformed into cage-like nanostructures. The morphology of

the composite nanostructures formed was octahedral.<sup>65</sup> Similarly, the *p*-MBA-functionalized Au nanorods were used for reactions with NMNCs such as [Au<sub>102</sub>(SR)<sub>44</sub>]<sup>13</sup> and [Au<sub>250</sub>(SR)<sub>*n*</sub>]<sup>42</sup> in a parallel way to generalize the process. But here less dense encapsulation of GNRs was noticed. It was suggested that some of these *p*-MBA-stabilized Au NCs would be deprotonated (i.e., S-PhCOONa) in the formation of the assembly. As a result, a few of the *p*-MBA ligands of these two NMNCs do not take part in the formation of H-bonds.

In yet another study, Bose et al. reported the reaction between a NMNC, [Au<sub>25</sub>(SR)<sub>18</sub>] (SR = 2-phenylethanethiol), and polydispersed silver NPs (~4 nm) capped with the same ligand.<sup>66</sup> The reaction produced alloyed NPs under ambient conditions. HRTEM study revealed that such type of reaction gave rise to highly monodisperse superlattices of 2D Au–Ag alloy NPs. Such reactions are highly dependent upon the nature of the capping ligands since reaction did not proceed when 4-(*tert*-butyl)benzyl mercaptan was used as a protecting ligand for the Au NCs.

Supracolloidal self-assembly of NMNCs, especially [Au<sub>102</sub>(*p*-MBA)<sub>44</sub>] under aqueous conditions, was studied by Nonappa and co-workers.<sup>67,68</sup> Monodisperse gold NCs were preferred for the formation of template-free 2D nanosheets and closed spherical capsids. Such supracolloidal self-assembly of [Au<sub>102</sub>(*p*-MBA)<sub>44</sub>] was obtained due to the presence of the spontaneous and inherent arrangement of the H-bonding interactions of *p*-MBA ligands. Dialysis of [Au<sub>102</sub>(*p*-MBA)<sub>44</sub>] (SR = S-PhCOOH or S-PhCOONa) from soluble water to insoluble methanol led to the formation of spontaneous self-assembly of such NMNCs into monolayer 2D sheets. The slow dialysis offered enough time for the NMNCs to assemble in the hexagonal close-packed structure as the geometry facilitates the formation of the maximum number of H-bonds. However, the rapid injection of dispersed partially deprotonated (in water) [Au<sub>102</sub>(*p*-MBA)<sub>44</sub>] into methanol resulted in spherical superstructures of an average diameter of 200 nm. The tomographic reconstruction data revealed that these superstructures were hollow. These hollow spherical superstructures were formed based on shape-defined NMNC subunits. These spherical superstructures were named “colloidal capsids” (see Figure 1 and section 4). The fusion of two capsids was also observed. The H-bonding interactions between two adjacent capsids could result in the fusion of two capsids. Ellipsoidal capsids were also formed either due to the rearrangement of defects upon assembly or fusion of two capsids. However, the forming mechanisms and how the ellipsoidal capsid shells can be tuned are currently unknown.

#### 5. SC OF NMNCs WITH OTHER MOLECULES

SC of NMNCs with other molecules such as fullerenes, cyclodextrins, cucurbiturils, crown ether, etc. is composed of special structural compatibility and host–guest interactions. In this section, we discuss such interactions one by one.

##### 5.1. SC of NMNCs with Fullerenes

Fullerenes are considered one of the important classes of molecules to explore SC because of their size, shape, rich  $\pi$ -electron cloud, and electron-accepting properties. Recently, Chakraborty et al. described the supramolecular functionalization of silver NMNCs with fullerenes.<sup>69</sup> Reaction between [Ag<sub>29</sub>(S<sub>2</sub>R)<sub>12</sub>]<sup>3-</sup> with C<sub>60</sub> at room temperature resulted in the generation of [Ag<sub>29</sub>(S<sub>2</sub>R)<sub>12</sub>(C<sub>60</sub>)<sub>*n*</sub>]<sup>3-</sup> ( $n = 1-9$ ). [Ag<sub>29</sub>(S<sub>2</sub>R)<sub>12</sub>]<sup>3-</sup> and four equivalents of C<sub>60</sub> gave rise to

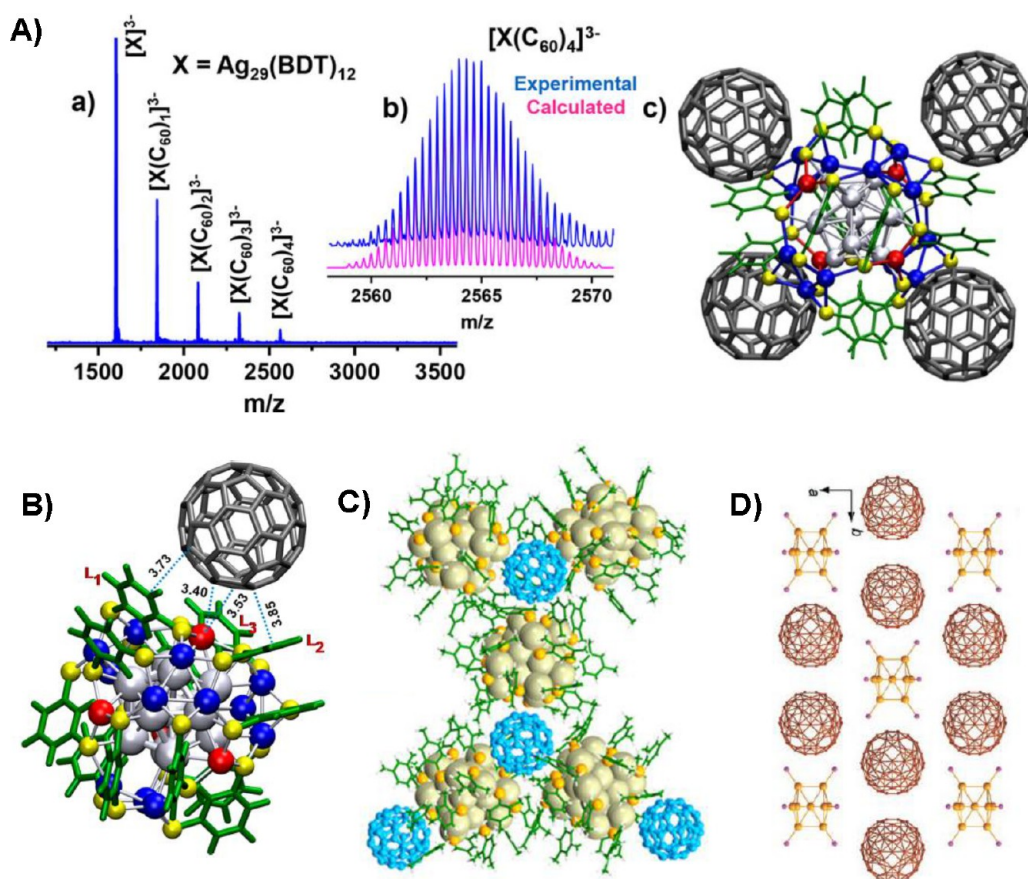


**Figure 8.** (A) (a) ESI-MS of  $[Ag_{29}(S_2R)_{12}(C_{60})_n]^{3-}$  ( $n = 1-4$ ) adducts. (b) Theoretical and experimental isotopic patterns of  $[Ag_{29}(S_2R)_{12}(C_{60})_4]^{3-}$ . (c) DFT optimized structure of  $[Ag_{29}(S_2R)_{12}(C_{60})_4]^{3-}$ . (B) Strong noncovalent interactions between the NMNC and  $C_{60}$ . (Reproduced from ref 69. Copyright 2018 American Chemical Society.) (C) Fullerene ( $C_{60}$ ) induced aggregation of  $[Ag_{25}(SR)_{18}]^-$ . (Adopted from the ref 70. Copyright 2020 American Chemical Society.) (D) Assembly of  $[Au_8(TPP)_8(C_{60})_2]$  along the (001) plane. (Reproduced from the ref 71. Copyright 2008 Wiley.)

$[Ag_{29}(S_2R)_{12}(C_{60})_n]^{3-}$  ( $n = 1-4$ ) complexes, which were detected by ESI-MS (Figure 8A). The ligand surfaces of the NMNC are organized in such a fashion to form a cavity, allowing the  $\pi$ -electrons of the surface of fullerenes to interact. Such host–guest complexations were enabled by this structural compatibility (Figure 8B). The structures of  $[Ag_{29}(S_2R)_{12}(C_{60})_n]^{3-}$  ( $n = 1-4$ ) adducts were predicted using molecular docking and DFT calculation. The non-covalent interactions such as  $\pi \cdots H-C$ ,  $\pi \cdots \pi$ , and vdWs interactions between the aromatic rings of  $S_2R$  of the NC and the aromatic surface of the fullerene were the main reason for the formation of such assemblies. Similar results were obtained when  $C_{70}$  was used in place of  $C_{60}$ . Similarly, fullerene ( $C_{60}$  and  $C_{70}$ ) based aggregation of  $[M_{25}(SR)_{18}]^-$  NCs ( $-SR =$  thiolate ligand,  $M = Ag$  or  $Au$ ) was also studied using ESI-MS.<sup>70</sup> The nature of the complexation witnessed in the case of  $[Ag_{29}(S_2R)_{12}]^{3-}$  was different compared to fullerene adducts of  $[M_{25}(SR)_{18}]^-$ . Multiple fullerenes interacted on the ligand surface of a single NMNC, in the case of  $[Ag_{29}(S_2R)_{12}]^{3-}$ . But multiple NMNCs interacted on the surface of a fullerene in the case of  $[M_{25}(SR)_{18}]^-$  (Figure 8C).

In another study, Schulz-Dobrick et al. reported the crystal structure of fullerides with Au NCs in 2008.<sup>71</sup> Single crystals were obtained via the layering method where slow interdiffusion of  $[(Au_8(TPP)_8)(NO_3)_2]$  in acetonitrile and  $KC_{60}$  in THF resulted in black crystals containing AuNCs and

fullerides (Figure 8D). By this method, two different complexes,  $[(Au_7(TPP)_7)C_{60} \cdot THF]$  and  $[(Au_8(TPP)_8)(C_{60})_2]$ , were obtained. Electrostatic attraction between fullerides and positively charged NMNCs and intermolecular interactions resulted in such intercluster building blocks. This kind of intercluster building block could bring in highly exciting properties such as electronic transport.

## 5.2. SC of NMNCs with Cyclodextrins

Cyclodextrin (CD) is a family of cyclic oligosaccharides containing a macrocyclic ring of glucose subunits (GS) connected by  $\alpha$ -1,4 glycosidic bonds. The three most studied CDs are  $\alpha$ -CD (connected by six GS),  $\beta$ -CD (connected by seven GS), and  $\gamma$ -CD (connected by eight GS). CD has a hydrophilic external surface and an inherent hydrophobic internal cavity. Due to these properties, it is known to produce supramolecular host–guest complexes.<sup>72</sup> In this section, we will mainly focus on the SC of CDs with NMNCs.

The supramolecular interaction between  $[Au_{25}(SBB)_{18}]$  ( $SBB = 4$ -*tert*-butylbenzyl mercaptan) and  $\beta$ -CDs was investigated by Pradeep and co-workers.<sup>72</sup> There were a maximum of four CDs on a single NC surface which were established by ESI-MS. Formation of such adducts is shown in Figure 9A. The supramolecular adducts,  $[Au_{25}(SBB)_{18} \cap \beta$ -CD $_n]$  ( $n = 1-4$ ), are presented in Figure 9B. DFT calculations suggested that host–guest interactions were favored through the finer rim of the CDs which was further recognized by

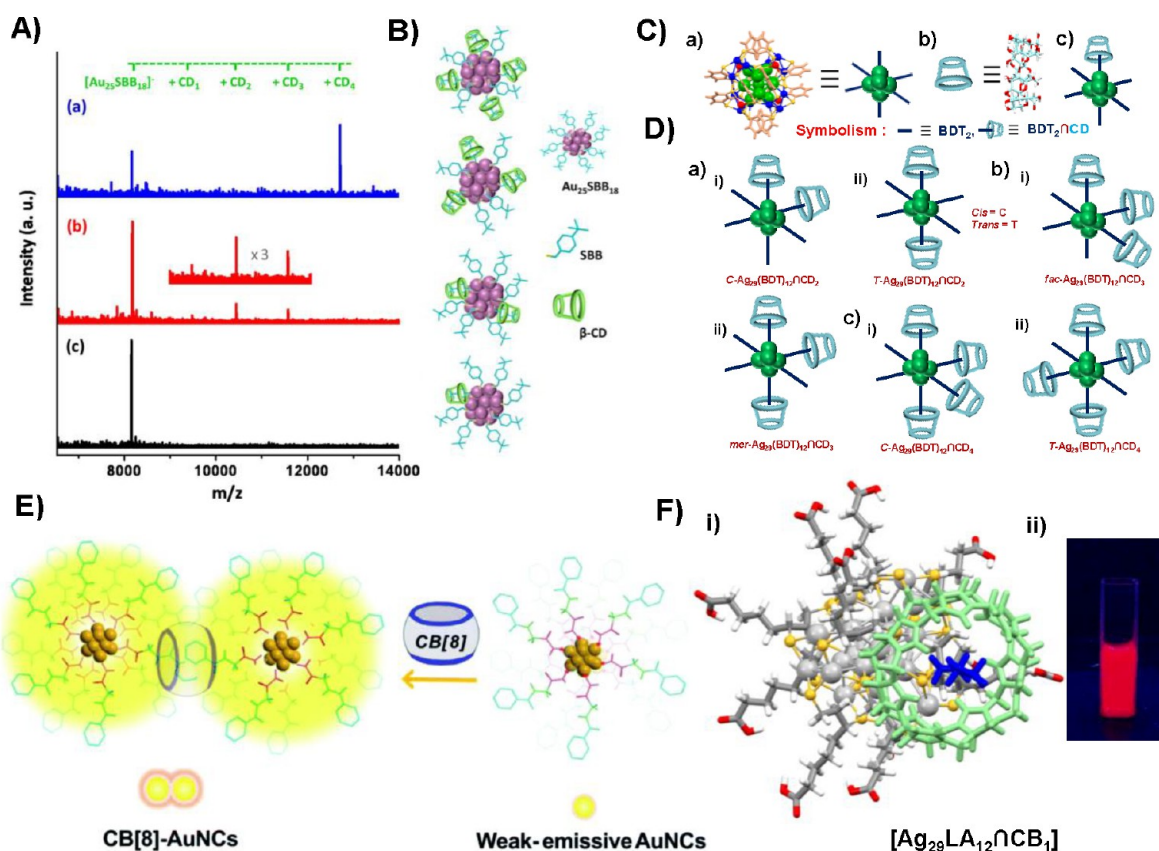


**Figure 9.** (A) ESI-MS of the  $[\text{Au}_{25}\text{SBB}_{18}\text{CD}_n]$  ( $n = 1-4$ ) adducts. (B) Schematic presentation of the  $[\text{Au}_{25}(\text{SBB})_{18}\text{CD}_n]$  ( $n = 1-4$ ) adducts. (Adopted from ref 72. Copyright 2014 American Chemical Society.) (C) Schematic presentation of (a)  $[\text{Ag}_{29}(\text{S}_2\text{R})_{12}]$  where  $\text{S}_2\text{R}$  is BDT and (b)  $\beta$ -CDs. (D) Simple presentation of the isomers of  $[\text{Ag}_{29}(\text{S}_2\text{R})_{12}\text{CD}_n]$  ( $n = 2$  to 3). (Reproduced from ref 81. Copyright 2018 American Chemical Society.) (E) Supramolecular interactions of CB[8] with AuNCs resulted in enhancement in luminescence. (Adopted from ref 82. Copyright 2020 Royal Society of Chemistry.) (F) (i) DFT optimized structure of  $[\text{Ag}_{29}(\text{LA})_{12}\text{CB}[7]_1]$ . (ii) Highly luminescent  $[\text{Ag}_{29}(\text{LA})_{12}\text{CB}[7]]$  complexes in water. (Reproduced from ref 85. Copyright 2020 American Chemical Society.)

optimizing the structure of  $\text{HSBB}\cap\beta\text{-CD}$  in DFT. The DFT optimized structure of  $[\text{Au}_{25}(\text{SBB})_{18}\text{CD}_4]$  revealed that the four  $\beta$ -CDs were attached with tetrahedral symmetry on the NMNC surface, reducing the steric hindrance among  $\beta$ -CDs. vdWs interactions between the SBB ligands and the  $\beta$ -CD were the main reason for the formation of such a complex. The noncovalent interactions between SBB and  $\beta$ -CD gave rise to an improvement of the luminescence and stability of the NMNC.

Similarly, Li and co-workers investigated the surface modification of  $[\text{Au}_{38}\text{S}_2(\text{SR})_{20}]$  ( $\text{SR}/\text{Adm} = 1$ -adamantane-thiolate) with  $\alpha$ -,  $\beta$ -, and  $\gamma$ -CDs using MS and UV-vis techniques.<sup>73</sup> Among all the CDs, only  $\beta$ -CDs were selectively chemisorbed onto the NMNC surface to form  $[\text{Au}_{38}\text{S}_2(\text{Adm})_{20}\text{CD}_1]$  and  $[\text{Au}_{38}\text{S}_2(\text{Adm})_{20}\text{CD}_2]$  complexes. The structures of these complexes were deciphered using molecular dynamics simulations where two  $\beta$ -CDs were attached at the two corners of the  $\text{Au}_{38}$  NC, reducing their mutual steric hindrance. The functionalization of  $\beta$ -CDs onto the NC surface resulted in stability. Similarly, Bhunia et al. also studied the supramolecular interactions of Au NCs capped by glutathione with  $\alpha$ -,  $\beta$ -, and  $\gamma$ -CDs.<sup>74</sup>

Isomerism in NMNCs is a highly interesting research theme.<sup>75-80</sup> In this context, supramolecular complexes,  $[\text{Ag}_{29}(\text{S}_2\text{R})_{12}\text{CD}_n]$  ( $n = 1$  to 6), were synthesized through the reaction between the as-prepared  $[\text{Ag}_{29}(\text{S}_2\text{R})_{12}]$  and  $\alpha$ -,  $\beta$ -, and  $\gamma$ -CDs in DMF.<sup>81</sup> ESI-MS and NMR study confirmed the

formation of supramolecular adducts. Molecular docking study and DFT calculations were carried out to obtain the lowest energy structures of  $[\text{Ag}_{29}(\text{S}_2\text{R})_{12}\text{CD}_n]$  ( $n = 1$  to 6) complexes which showed that a pair of  $\text{S}_2\text{R}$  ligands were encapsulated by CD. The  $\pi\cdots\text{H}-\text{C}$ , hydrogen bonding, weak ionic  $\text{Ag}\cdots\text{O}$ , and vdWs interactions play a crucial role to form such supramolecular adducts. More significantly, the geometries of these supramolecular complexes resembled the octahedral complexes of transition metals, giving rise to different isomers. A simple representation of the isomers is presented in Figure 9C and D. Such kind of isomers were separated using IM MS.<sup>81</sup>

### 5.3. SC of NMNCs with Cucurbiturils

Cucurbiturils are supramolecular macrocyclic molecules consisting of glycoluril ( $=\text{C}_4\text{H}_2\text{N}_4\text{O}_2=$ ) monomers connected by methylene bridges ( $-\text{CH}_2-$ ). The crystal structures of cucurbiturils revealed that the O atoms are situated along the edges and tilted inward, creating a partly enclosed cavity. The name of this molecule is derived from its resemblance with a pumpkin of the Cucurbitaceae family. Cucurbiturils are generally written as cucurbit[ $n$ ]uril, where  $n$  is the number of glycoluril ( $=\text{C}_4\text{H}_2\text{N}_4\text{O}_2=$ ) units. Two simple abbreviations are  $\text{CB}[n]$  and  $\text{CB}_n$ . These compounds are suitable hosts for an array of neutral and cationic species through hydrophobic interactions and cation-dipole interactions, respectively. Here,

we discuss mainly the supramolecular complexes of CBs with NMNCs.

Recently, Jiang et al. developed a method to reversibly brighten and enhance the emission of a gold NC,  $[\text{Au}_{22}(\text{FGGC})_{18}]$  (N-terminal Phe-Gly-Gly-Cys peptide = FGGC), using supramolecular complexation between FGGC peptides and  $\text{CB}[n]$  ( $n = 7, 8$ ) in water (Figure 9E).<sup>82</sup> This is the first report of supramolecular complexation of a NMNC with CBs. The approach of supramolecular complexation effectively enhanced the emission of AuNCs by rigidifying the ligand surface of an NMNC. As a result, an effective restriction of the nonradiative transition and elevation of the radiative transition occurred which was confirmed using an ultrafast spectroscopy study. The supramolecular interaction between the NMNCs and CBs resulted in a high QY of 51% for CB[7] and 39% for CB[8] in water at room temperature, respectively.

In another study, Pradeep and co-workers investigated the formation of supramolecular host–guest complexation of  $[\text{Ag}_{29}(\text{LA})_{12}]$ <sup>83,84</sup> (LA =  $\alpha$ -lipoic acid) with CB[7] in an aqueous medium at room temperature (Figure 9F).<sup>85</sup> Molecular docking study and DFT calculations were used to support the experimental results. This study demonstrated the encapsulation of LA ligands by CB[7]. Here also, inclusion complexation leads to improved luminescence of about 1.25 times compared to the parent NMNC.

#### 5.4. SC of NMNCs with Crown Ethers

Crown ethers are heterocyclic compounds containing several ether groups. They were highly used to form supramolecular host–guest complexes. The hydrophilic cavity created by ether oxygen atoms is highly efficient to capture alkali and alkaline earth metal ions. The cavity size is highly specific for a specific metal ion. For example, 18-crown-6, 15-crown-5, and 12-crown-4 have a high affinity for potassium cation, sodium cation, and lithium cation, respectively. The hydrophilic cavity is surrounded by the hydrophobic ethylenic groups. Crown ethers are well-known for the ion transport mechanism and phase-transfer catalysis. They are used as building blocks for supramolecular architectures.

Pradeep and co-workers reported the first crystal structure of a supramolecular assembly of a silver NC,  $[\text{Ag}_{29}(\text{S}_2\text{R})_{12}(\text{TPP})_4]^{3-}$  ( $\text{Ag}_{29}$ ), with dibenzo-18-crown-6 ( $\text{DB}_{18}\text{C}_6$ ) using SCXRD (Figure 10A).<sup>86</sup> The crystallization induced self-arrangement of  $\text{DB}_{18}\text{C}_6$  molecules produced a hexamer cagelike structure in the interstitial spaces of the crystal lattice of trigonal  $\text{Ag}_{29}$  ( $\text{Ag}_{29}\text{T}$ ) NCs. Such insertion of hexameric cages in the crystal lattice gave rise to an anisotropic expansion of the  $\text{Ag}_{29}\text{T}$  lattice along its  $z$ -axis. The presence of intermolecular  $\pi\cdots\text{H}-\text{C}$  interactions between  $\text{DB}_{18}\text{C}_6\text{Na}^+$  and the TPP and  $\text{S}_2\text{R}$  ligands of the NC and electrostatic interaction between 3  $\text{DB}_{18}\text{C}_6\text{Na}^+$  and the negatively charged  $\text{Ag}_{29}$  NC was the main reason for such self-organized assemblies (Figure 10B). The distance between the sodium ions is also provided in Figure 10C. This structure resembles a new family of “lattice inclusion” complexes in NMNCs. Assembly of NMNCs with  $\text{DB}_{18}\text{C}_6\text{Na}^+$  is presented in Figure 10D. Such supramolecular interactions resulted in  $\sim 3.5$  times improvement in luminescence compared to the parent crystals,  $\text{Ag}_{29}\text{T}$ . Such kind of study delivers an approach for building new NC-assembled hybrid materials with enhanced properties.

#### 5.5. Other Supramolecular Interactions of NMNCs

Muhammed and co-workers recently functionalized AgNCs with a pillar[5]arene based host ligand ( $\text{P}_5$ )  $[\text{Ag}_{29}(\text{LA}-$

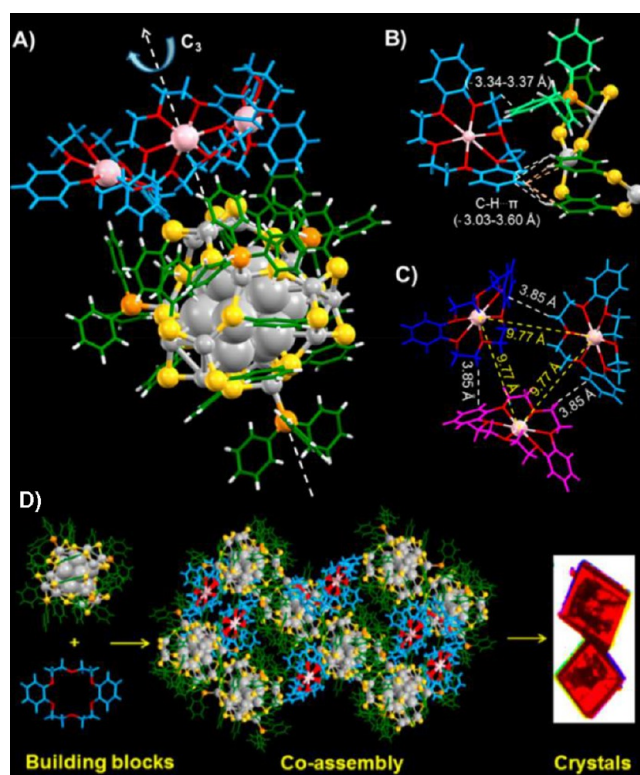


**Figure 10.** (A) Crystal structure of  $[\text{Ag}_{29}(\text{S}_2\text{R})_{12}(\text{TPP})_4]^{3-}$  with dibenzo-18-crown-6. (B) Supramolecular interaction between one of the  $\text{DB}_{18}\text{C}_6\text{Na}^+$  and  $\text{S}_2\text{R}$  and TPP of the NMNC. (C) Zoomed in view of the three  $\text{DB}_{18}\text{C}_6\text{Na}^+$  molecules connected to the NMNC. Color codes: Ag, gray; S, yellow; P, orange; O, red; C of TPP and  $\text{S}_2\text{R}$ , green; H of TPP and  $\text{S}_2\text{R}$ , white; H and C of  $\text{DB}_{18}\text{C}_6$ , light blue; Na, pink. Color codes in part C: C and H of the three  $\text{DB}_{18}\text{C}_6\text{Na}^+$  molecules, light blue, dark blue, and purple, respectively. (D) Formation of coassembly of  $[\text{Ag}_{29}(\text{S}_2\text{R})_{12}(\text{TPP})_4]^{3-}$  with dibenzo-18-crown-6 via supramolecular interactions. (Adopted from ref 86. Copyright 2019 American Chemical Society.)

$\text{P}_5)_{12}(\text{TPP})_2]$  (LA- Lipoic acid).<sup>87</sup> The AgNCs were synthesized in two different ways: (i) via direct synthesis using silver nitrate salt ( $\text{AgNO}_3$ ), LA- $\text{P}_5$ , and TPP and (ii) via the reaction between  $[\text{Ag}_{18}\text{H}_{16}(\text{TPP})_{10}]_2^+$  (ref 88) and LA- $\text{P}_5$  (Figure 11A). The pillar[5]arene based NMNCs  $[\text{Ag}_{29}(\text{LA}-\text{P}_5)_{12}(\text{TPP})_2]$  showed a reversible host–guest interaction with neutral alkylamines and cationic quaternary ammonium guests (Figure 11B). This supramolecular interaction resulted in the formation of spherical assemblies with a dramatic enhancement of luminescence by  $\sim 2000$ -fold. This is the highest luminescence enhancement data reported in the literature to date for NMNCs.

In another study, Mohammed and co-workers explored the charge-transfer dynamics between the positively charged 5,10,15,20-tetra(1-methyl-4-pyridino)-porphyrin tetra(p-toluene sulfonate) (TMPyP) and negatively charged undoped and Au-doped  $\text{Ag}_{29}$  NMNCs.<sup>89</sup> Transient absorption (TA) spectroscopic study revealed that the interfacial charge transfer, the triplet state lifetime, and the intersystem crossing of porphyrin can be altered by the doping of gold in  $\text{Ag}_{29}$  NCs. Moreover, the electrostatic interaction between the negatively charged NMNCs and the positively charged TMPyP played a key role in the complex formation and subsequently facilitated the transfer process.

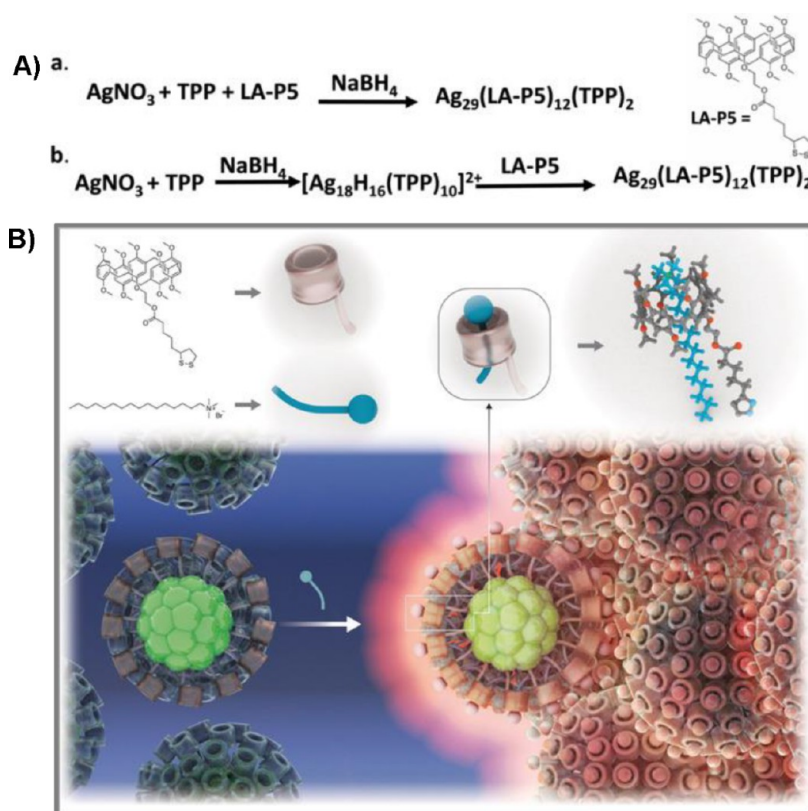


**Figure 11.** (A) Synthesis of  $[\text{Ag}_{29}(\text{LA-P5})_{12}(\text{TPP})_2]$  via two methods: (i) direct synthesis and (ii) ligand exchange. (B) Schematic representation of host–guest interaction between  $[\text{Ag}_{29}(\text{LA-P5})_{12}(\text{TPP})_2]$  and CTAB leading to self-assembly and luminescence enhancement. (Reproduced from ref 87. Copyright 2019 Wiley.)

## 6. PROPERTIES OF SUPRAMOLECULAR ASSEMBLIES OF NMNCs

Supramolecular complexes generally should have the following basic properties:

- (1) Structural complementarity: The geometric structure and electronic properties of the host and guest are mutually complementing. Complementarity permits the host to accomplish a selective binding of the guest of a specific structure only. This phenomenon is termed as “molecular recognition” in supramolecular chemistry.
- (2) Supramolecular complexes have a high structural orientation because of the presence of a large number of noncovalent interactions.
- (3) The supramolecular interactions could result in self-assembled structures. In this process, small molecular species spontaneously interact together and result in much larger and complex assemblies. As a result, the entropy of the system reduces, or  $\Delta S < 0$ . However, the process is spontaneous, so the Gibbs energy is negative:  $\Delta G = \Delta H - T\Delta S < 0$ . This must be true if  $\Delta H < 0$  and  $|\Delta H| > |T\Delta S|$ . So, self-assembly is accompanied by the release of large amounts of heat.

Apart from all these basic properties, many other properties are also evidenced for the supramolecular complexes of NMNCs which are discussed below.

### 6.1. Mechanical

The mechanical properties of NMNC-assembled solids generated from the supramolecular self-assembly are beginning to be explored. Pradeep and co-workers explored the

mechanical properties of single crystals of NMNCs such as  $\text{Ag}_{29}$  polymorphs ( $\text{Ag}_{29}$  C and  $\text{Ag}_{29}$  T, respectively), monothiol-protected  $\text{Ag}_{46}$ , and its cocrystal with  $\text{Ag}_{40}$  crystallizing in trigonal and monoclinic lattices ( $\text{Ag}_{46}$  T and  $\text{Ag}_{40/46}$  M), respectively (Figure 12A).<sup>90</sup> The acquired Young’s modulus ( $E_r$ ) values of the NC-assembled solids were comparable to those of zeolitic imidazolate frameworks (ZIFs). The data exhibited the following trend:  $\text{Ag}_{29}$  T >  $\text{Ag}_{29}$  C >  $\text{Ag}_{40/46}$  M >  $\text{Ag}_{46}$  T. The viscoelastic properties of all of the four NC-assembled solids were evaluated, and the value of the  $\tan \delta$ /damping factor of  $\text{Ag}_{46}$  T was higher than those of other systems. The study concluded that the supramolecular interactions of the NMNCs’ surfaces playing a key to influencing the mechanical properties.

### 6.2. Luminescence

Supramolecular complexation of NMNCs could result in enhancement of luminescence. Enhancement of luminescence was evidenced for CBs, CDs, and crown ethers when they formed supramolecular adducts with NMNCs.<sup>85,86</sup> Due to the presence of strong noncovalent interactions between the host and guest, the whole system becomes highly rigid. As a result, the whole system experienced a high luminescence. Similar luminescence enhancement was observed for  $\text{Ag}_{29}$  C compared to  $\text{Ag}_{29}$  T.<sup>53</sup>

### 6.3. Charge Transfer

There could be charge transfer between the guest and host if they differ in their electronic properties. This phenomenon was evidenced in the case of  $[\text{Ag}_{29}(\text{S}_2\text{R})_{12}(\text{C}_{60})_n]^{3-}$ , where NMNC has three negative charge states.<sup>69</sup> Collision induced dissociation (CID) study revealed that the NMNC transferred

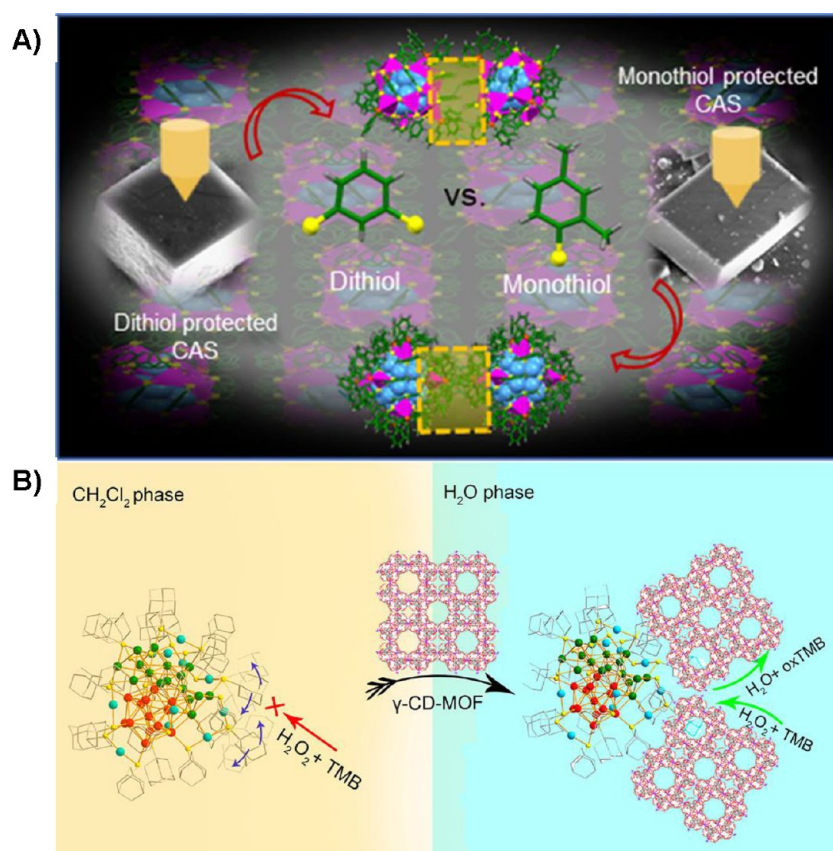


**Figure 12.** (A) Study of the mechanical properties of single crystals of NMNCs such as dithiol-protected  $\text{Ag}_{29}$  polymorphs (C and T), monothiol-protected  $\text{Ag}_{46}$ , and its cocrystal with  $\text{Ag}_{40}$ . (Reproduced from ref 90. Copyright 2020 American Chemical Society.) (B)  $\gamma$ -CD-MOF induced water solubility of  $[\text{Au}_{40}(\text{S-Adm})_{22}]$  NMNCs. This water-soluble hybrid component activated gold NCs for the horseradish peroxidase (HRP)-mimicking catalysis. (Adopted from ref 98. Copyright 2020 American Chemical Society.)

an electron to  $\text{C}_{60}$ . Similarly, the reducing NC  $[\text{Ni}_9\text{Te}_6(\text{PET}_3)_8]$  is known to form a charge-transfer complex with the fullerene.<sup>91</sup> Microcrystals of  $\text{Au}_{32}(\text{Bu}_3\text{P})_{12}\text{Cl}_8$  NCs containing highly ordered self-assembly ( $\sigma = 1.56 \times 10^{-4}$  S/m) exhibited enhanced charge carrier transport by 2 orders of magnitude compared to polycrystalline thin films ( $\sigma \approx 1 \times 10^{-6}$  S/m).<sup>92</sup>

#### 6.4. Magnetic

The magnetic property of the NC is a very recent emerging field. Supramolecular complexes of NCs could result in an enhancement in the magnetic property. Binary assemblies of fullerenes with  $[\text{Ni}_9\text{Te}_6(\text{PET}_3)_8]$  transition metal NCs experienced magnetic properties at low temperatures.<sup>91</sup>

## 7. APPLICATIONS OF SUPRAMOLECULAR ASSEMBLIES OF NMNCs

Various applications of supramolecular complexes of NMNCs are pointed out in the following:

### 7.1. Sensing

Sensing is one of the fundamental applications of NMNCs. Supramolecular complexes of  $[\text{Ag}_{29}\text{LA}_{12}]$  with CDs displayed red luminescence. In recent studies, Nag et al. have developed a method to sense dopamine at a concentration as low as 10 nM using  $[\text{Ag}_{29}\text{LA}_{12}@\text{CD}_n]$  ( $n = 1-3$ ).<sup>85</sup> Supramolecular complexes of  $[\text{Ag}_{29}\text{LA}_{12}]$  with CDs are highly red luminescent. The dopamine molecules were encapsulated by the vacant cavity of CD, which resulted in quenching of the luminescence. Recently, the rapid and cyclic detection of explosives such as

nitrobenzene (NB) was performed using a hybrid polymer membrane generated from  $[\text{Ag}_{12}(\text{StBu})_6(\text{CF}_3\text{COO})_6(\text{NH}_2\text{-bpz})_3]_n$ -MOF  $[\text{NH}_2\text{-Ag}_{12}\text{bpz}]$ .<sup>93</sup> The chiral recognition of D- and L-Trp (Trp = tryptophan) was reported using the assembled enantiomeric  $[\text{Au}_{14}(\text{MPA})_6(\text{D/L-Trp})_4]$  NMNCs generated by  $\text{Zn}^{2+}$  coordination (MPA = 3-mercaptopropionic acid).<sup>94</sup>

### 7.2. Cell Imaging

Live cell imaging is one of the fascinating applications of supramolecular complexes of NMNCs. Recently, supramolecular complexes of  $[\text{Au}_{22}(\text{FGGC})_{18}]$  with CB[7] exhibited exceptional imaging of cancer A549 cells.<sup>82</sup> Also, cancer cell imaging, targeted delivery, and photothermal/photodynamic therapies were reported using  $[\text{Pt}_1\text{Ag}_{28}]$  NC assembly.<sup>95</sup> Further, a folic acid based  $[\text{Au}_{22}(\text{SG})_{18}]$  NMNC assembly has been utilized to study the cancer cells.<sup>96</sup>

### 7.3. Photocatalytic Activity

Xie and co-workers introduced a hybrid material, consisting of per-6-thio- $\beta$ -cyclodextrin (SH- $\beta$ -CD) capped gold NCs and  $\text{TiO}_2$  NPs.<sup>97</sup> This hybrid material displayed improved photocatalytic performance over  $\text{TiO}_2$  NPs. The hybrid material exhibited enhanced effects on photocatalytic decomposition of organic pollutants via host-guest complexation. This hybrid  $\text{TiO}_2$  system had better efficiency ( $\sim 98\%$ ) compared to only  $\text{TiO}_2$  NPs ( $\sim 47\%$ ).

#### 7.4. Catalytic Activity

Zhao et al. recently generated a hybrid material using adamantanethiolate-protected  $[\text{Au}_{40}(\text{S-Adm})_{22}]$  NMNCs and  $\gamma$ -CD-MOF.<sup>98</sup> This hybrid material exhibited excellent water solubility and catalytic activity which is different from the parent  $[\text{Au}_{40}(\text{S-Adm})_{22}]$  NMNCs (Figure 12B). This water-soluble hybrid component activated gold NCs for the horseradish peroxidase (HRP)-mimicking catalysis.

#### 7.5. Other Applications

Cluster-assembled solids have been utilized to generate multicolor light-emitting diodes (LEDs), where NMNCs' assembly acts as a color conversion layer. Wu et al. effectively established the construction of LEDs using an assembly of  $[\text{Cu}_{14}(\text{DT})_{10}]$  (DT-1-dodecanethiol).<sup>99</sup> Fabrication of a WLED (white light-emitting diode) using a Zn-coordinated NMNCs' assembly  $[\text{Zn-Au@SG}]$  was reported (SG = glutathiolate).<sup>100</sup>

### 8. CONCLUSIONS AND FUTURE PERSPECTIVES

This Review highlights the various supramolecular assemblies of NMNCs in gaseous, solution, and solid states. Intercluster reaction, dimerization, cation induced dimerization, and ligand–NC interactions were discussed in the context of supramolecular interactions of NMNCs in gaseous and solution phases. In the solid state, interactions, chirality, and symmetry were studied in crystal lattices. These were mostly studied by SCXRD and electron microscopy. This work also presented the SC of NMNCs with molecules such as (i) fullerenes, (ii) CDs, (iii) CBs, and (iv) crown ethers. Structural compatibility between the NMNCs and such molecules favors host–guest complexes.

There are many challenges in this field. In the initial stages of NMNC research, understanding the core, ligands, and total structures of clusters themselves was of interest to the community rather than the understanding of NMNC–NMNC interactions. It is natural that science in this area evolved this way. Nowadays, the community is interested in exploring NMNC assemblies of such large molecules in greater detail within their crystal lattices. However, the nature of supramolecular interactions in NMNC crystals is difficult to be understood at the same level of precision as in the case of organic molecules as most structures are solved by excluding counterions and solvents. In many cases, solvent molecules are not present in the solved crystal structures. Even finding a counterion is very difficult.<sup>18</sup> They are often observed in other studies such as infrared spectroscopy or mass spectrometry. Although such supramolecular interactions in crystal structures are not studied in greater detail, in  $\text{Ag}_{44}(\text{MBA})_{30}$ , for example, such interactions between ligands have been shown to be the fundamental reason for crystal assembly.<sup>20</sup> Generally, the resolution of such molecular crystals is lower than that of small organic and inorganic molecules.<sup>13,54</sup> It is clear that the dynamic nature of NMNCs makes it difficult to form stable directional assemblies in most of them. Besides, each NMNC is stable only in a few specific solvents. Thus, exploring crystallization under common conditions cannot be attempted for all NMNCs.

Supramolecular interactions of NMNCs are largely about the interactions of ligands. One can find supramolecular interactions in all condensed phases. However, in the case of NMNCs, new properties such as luminescence enhancement, mechanical properties, electrical conductivity, etc. may arise

due to such supramolecular assemblies. With the help of such supramolecular assemblies one can develop new hybrid nanomaterials allowing noncovalent interactions. It is a highly interdisciplinary research area. Much emphasis on the crystal structures was given in many studies to understand the systems properly. Such assemblies lead to highly complex structures, and some of the structures are comparable to  $\alpha$ -helices and  $\beta$ -sheets of proteins.<sup>47</sup>

Noble metals such as silver and gold are highly expensive. However, some of the luminescent NMNCs are biocompatible and are used for cell imaging.<sup>1,2</sup> Some of them are well-known for catalysis.<sup>1,2</sup> Recently, there is interest in synthesizing copper NCs which may turn out to be cheaper.

Despite these limitations, there are many possibilities for future work:

- (i) Intercluster assembly could induce new properties such as mechanical, optical, and magnetic properties as well as gas sensing and storage.
- (ii) CD, CB, and porphyrins based NMNC-assembled solids can be potential candidates for gas storage and sensing. NC based host–guest interactions are still a growing research area compared to intracuster growth and intercluster assembly. Noncovalent interactions between hosts and guests could alter the electronic and geometric structures and properties of individual NMNCs. Till now only very few examples have been reported. Supramolecular interactions could result in the enhancement of luminescence.
- (iii) Although some of the supramolecular complexes were characterized as a mixture of adducts in the solution and gas phases, isolation of these complexes in the solid state can give rise to a new class of NMNC-assembled solids. Moreover, separation of the isomers of these supramolecular complexes due to the different binding modes of NMNCs is challenging. Such isomerism could result in various novel properties such as chirality, self-assembly, etc.
- (iv) There are large possibilities to extend these supramolecular complexes to NMNC-assembled metal–organic frameworks and polyoxometalates.<sup>101</sup> Such kind of supramolecular complexes may give rise to new examples of magnetic and conductive luminescent materials.
- (v) Supramolecular complexes of NMNCs with CDs and CBs could be utilized as drug delivery agents and for bioimaging.
- (vi) Studies such as dynamic light scattering, small angle X-ray scattering, small angle neutron scattering, etc. could be used to analyze the supramolecular complexes of NMNCs in the immediate future.
- (vii) Roy et al. demonstrated a binary assembly of fullerenes with transition metal NCs.<sup>91,102,103</sup> Similar kinds of studies can be performed for other atomically precise NC systems such as metal oxides, polyoxometalates, metal peroxides, boron oxides, and boron clusters, which are also atomically precise.
- (viii) CDs, CBs, and fullerenes can be used as linkers between NCs and other atomically precise NC systems such as metal oxides, polyoxometalates, metal peroxides, boron oxides, and boron clusters. This could result in hybrid nanomaterials with enhanced properties.

It is clear that these and other related aspects will enrich the area in the years to come.

## AUTHOR INFORMATION

### Corresponding Author

**Thalappil Pradeep** – DST Unit of Nanoscience (DST UNS) and Thematic Unit of Excellence, Department of Chemistry, Indian Institute of Technology Madras, Chennai 600036, India; [orcid.org/0000-0003-3174-534X](https://orcid.org/0000-0003-3174-534X); Email: [pradeep@iitm.ac.in](mailto:pradeep@iitm.ac.in); Fax: +91-44 2257-0545

### Author

**Abhijit Nag** – DST Unit of Nanoscience (DST UNS) and Thematic Unit of Excellence, Department of Chemistry, Indian Institute of Technology Madras, Chennai 600036, India; Present Address: A.N.: University of Edinburgh, Joseph Black Building, David Brewster Road, Edinburgh EH93FJ, Scotland

Complete contact information is available at:

<https://pubs.acs.org/10.1021/acsnanoscienceau.1c00046>

### Notes

The authors declare no competing financial interest.

## ACKNOWLEDGMENTS

We thank the Department of Science and Technology, Government of India for constantly supporting our research program on nanomaterials. A.N. thanks IIT Madras for a Postdoctoral fellowship. T.P. acknowledges support from the Centre of Excellence on Molecular Materials and Functions under the Institution of Eminence scheme of IIT Madras.

## REFERENCES

- (1) Chakraborty, I.; Pradeep, T. Atomically Precise Clusters of Noble Metals: Emerging Link between Atoms and Nanoparticles. *Chem. Rev.* **2017**, *117* (12), 8208–8271.
- (2) Jin, R.; Zeng, C.; Zhou, M.; Chen, Y. Atomically Precise Colloidal Metal Nanoclusters and Nanoparticles: Fundamentals and Opportunities. *Chem. Rev.* **2016**, *116* (18), 10346–10413.
- (3) Takano, S.; Ito, S.; Tsukuda, T. Efficient and Selective Conversion of Phosphine-Protected (MAu8)2+ (M = Pd, Pt) Superatoms to Thiolate-Protected (MAu12)6+ or Alkynyl-Protected (MAu12)4+ Superatoms via Hydride Doping. *J. Am. Chem. Soc.* **2019**, *141* (40), 15994–16002.
- (4) Hirata, K.; Chakraborty, P.; Nag, A.; Takano, S.; Koyasu, K.; Pradeep, T.; Tsukuda, T. Interconversions of Structural Isomers of [PdAu8(PPh3)8]2+ and [Au9(PPh3)8]3+ Revealed by Ion Mobility Mass Spectrometry. *J. Phys. Chem. C* **2018**, *122* (40), 23123–23128.
- (5) Ghosh, A.; Bodiuzzaman, M.; Nag, A.; Jash, M.; Baksi, A.; Pradeep, T. Sequential Dihydrogen Desorption from Hydride-Protected Atomically Precise Silver Clusters and the Formation of Naked Clusters in the Gas Phase. *ACS Nano* **2017**, *11* (11), 11145–11151.
- (6) Ito, S.; Takano, S.; Tsukuda, T. Alkynyl-Protected Au22(C≡CR)18 Clusters Featuring New Interfacial Motifs and R-Dependent Photoluminescence. *J. Phys. Chem. Lett.* **2019**, *10* (21), 6892–6896.
- (7) Guan, Z.-J.; Hu, F.; Li, J.-J.; Wen, Z.-R.; Lin, Y.-M.; Wang, Q.-M. Isomerization in Alkynyl-Protected Gold Nanoclusters. *J. Am. Chem. Soc.* **2020**, *142* (6), 2995–3001.
- (8) Alhilaly, M. J.; Bootharaju, M. S.; Joshi, C. P.; Besong, T. M.; Emwas, A.-H.; Juarez-Mosqueda, R.; Kaappa, S.; Malola, S.; Adil, K.; Shkurenko, A.; Häkkinen, H.; Eddaoudi, M.; Bakr, O. M. [Ag67-(SPhMe2)32(PPh3)8]3+: Synthesis, Total Structure, and Optical Properties of a Large Box-Shaped Silver Nanocluster. *J. Am. Chem. Soc.* **2016**, *138* (44), 14727–14732.
- (9) Ghosh, A.; Ghosh, D.; Khatun, E.; Chakraborty, P.; Pradeep, T. Unusual reactivity of dithiol protected clusters in comparison to monothiol protected clusters: studies using Ag51(BDT)19(TPP)3 and Ag29(BDT)12(TPP)4. *Nanoscale* **2017**, *9* (3), 1068–1077.
- (10) Bodiuzzaman, M.; Ghosh, A.; Sugi, K. S.; Nag, A.; Khatun, E.; Varghese, B.; Paramasivam, G.; Antharjanam, S.; Natarajan, G.; Pradeep, T. Camouflaging Structural Diversity: Co-crystallization of Two Different Nanoparticles Having Different Cores But the Same Shell. *Angew. Chem., Int. Ed.* **2019**, *58* (1), 189–194.
- (11) Zhu, M.; Aikens, C. M.; Hollander, F. J.; Schatz, G. C.; Jin, R. Correlating the Crystal Structure of A Thiol-Protected Au25 Cluster and Optical Properties. *J. Am. Chem. Soc.* **2008**, *130* (18), 5883–5885.
- (12) Heaven, M. W.; Dass, A.; White, P. S.; Holt, K. M.; Murray, R. W. Crystal Structure of the Gold Nanoparticle [N(C8H17)4][Au25-(SCH2CH2Ph)18]. *J. Am. Chem. Soc.* **2008**, *130* (12), 3754–3755.
- (13) Jadzinsky, P. D.; Calero, G.; Ackerson, C. J.; Bushnell, D. A.; Kornberg, R. D. Structure of a Thiol Monolayer-Protected Gold Nanoparticle at 1.1 Å Resolution. *Science* **2007**, *318* (5849), 430.
- (14) Qian, H.; Jin, R. Controlling Nanoparticles with Atomic Precision: The Case of Au144(SCH2CH2Ph)60. *Nano Lett.* **2009**, *9* (12), 4083–4087.
- (15) Fields-Zinna, C. A.; Sardar, R.; Beasley, C. A.; Murray, R. W. Electrospray Ionization Mass Spectrometry of Intrinsically Cationized Nanoparticles, [Au144/146(SC11H22N(CH2CH3)3)x(S(CH2)5CH3)y]x+. *J. Am. Chem. Soc.* **2009**, *131* (44), 16266–16271.
- (16) Zeng, C.; Chen, Y.; Liu, C.; Nobusada, K.; Rosi, N. L.; Jin, R. Gold tetrahedra coil up: Kekulé-like and double helical superstructures. *Sci. Adv.* **2015**, *1* (9), e1500425.
- (17) Qian, H.; Eckenhoff, W. T.; Zhu, Y.; Pintauer, T.; Jin, R. Total Structure Determination of Thiolate-Protected Au38 Nanoparticles. *J. Am. Chem. Soc.* **2010**, *132* (24), 8280–8281.
- (18) AbdulHalim, L. G.; Bootharaju, M. S.; Tang, Q.; Del Gobbo, S.; AbdulHalim, R. G.; Eddaoudi, M.; Jiang, D.-e.; Bakr, O. M. Ag29(BDT)12(TPP)4: A Tetravalent Nanocluster. *J. Am. Chem. Soc.* **2015**, *137* (37), 11970–11975.
- (19) Joshi, C. P.; Bootharaju, M. S.; Alhilaly, M. J.; Bakr, O. M. [Ag25(SR)18]–: The “Golden” Silver Nanoparticle. *J. Am. Chem. Soc.* **2015**, *137* (36), 11578–11581.
- (20) Yoon, B.; Luedtke, W. D.; Barnett, R. N.; Gao, J.; Desireddy, A.; Conn, B. E.; Bigioni, T.; Landman, U. Hydrogen-bonded structure and mechanical chiral response of a silver nanoparticle superlattice. *Nat. Mater.* **2014**, *13* (8), 807–811.
- (21) Tofanelli, M. A.; Ni, T. W.; Phillips, B. D.; Ackerson, C. J. Crystal Structure of the PdAu24(SR)180 Superatom. *Inorg. Chem.* **2016**, *55* (3), 999–1001.
- (22) Takano, S.; Tsukuda, T. Chemically Modified Gold/Silver Superatoms as Artificial Elements at Nanoscale: Design Principles and Synthesis Challenges. *J. Am. Chem. Soc.* **2021**, *143* (4), 1683–1698.
- (23) Chakraborty, P.; Pradeep, T. The emerging interface of mass spectrometry with materials. *NPG Asia Mater.* **2019**, *11* (1), 48.
- (24) Bodiuzzaman, M.; Dar, W. A.; Pradeep, T. Cocrystals of Atomically Precise Noble Metal Nanoclusters. *Small* **2021**, *17* (27), 2003981.
- (25) Khatun, E.; Pradeep, T. New Routes for Multicomponent Atomically Precise Metal Nanoclusters. *ACS Omega* **2021**, *6* (1), 1–16.
- (26) Krishnadas, K. R.; Sementa, L.; Medves, M.; Fortunelli, A.; Stener, M.; Fürstenberg, A.; Longhi, G.; Bürgi, T. Chiral Functionalization of an Atomically Precise Noble Metal Cluster: Insights into the Origin of Chirality and Photoluminescence. *ACS Nano* **2020**, *14* (8), 9687–9700.
- (27) Zeng, Y.; Havenridge, S.; Gharib, M.; Baksi, A.; Weerawardene, K. L. D. M.; Zieffuß, A. R.; Strelow, C.; Rehbock, C.; Mews, A.; Barcikowski, S.; Kappes, M. M.; Parak, W. J.; Aikens, C. M.; Chakraborty, I. Impact of Ligands on Structural and Optical Properties of Ag29 Nanoclusters. *J. Am. Chem. Soc.* **2021**, *143* (25), 9405–9414.



- (28) Chakraborty, P.; Nag, A.; Chakraborty, A.; Pradeep, T. Approaching Materials with Atomic Precision Using Supramolecular Cluster Assemblies. *Acc. Chem. Res.* **2019**, *52* (1), 2–11.
- (29) Rival, J. V.; Mymona, P.; Lakshmi, K. M.; Nonappa; Pradeep, T.; Shibu, E. S. Self-Assembly of Precision Noble Metal Nanoclusters: Hierarchical Structural Complexity, Colloidal Superstructures, and Applications. *Small* **2021**, *17* (27), 2005718.
- (30) Bonacchi, S.; Antonello, S.; Dainese, T.; Maran, F. Atomically Precise Metal Nanoclusters: Novel Building Blocks for Hierarchical Structures. *Chem.—Eur. J.* **2021**, *27* (1), 30–38.
- (31) Li, Y.; Zhou, M.; Song, Y.; Higaki, T.; Wang, H.; Jin, R. Double-helical assembly of heterodimeric nanoclusters into supercrystals. *Nature* **2021**, *594* (7863), 380–384.
- (32) Krishnadas, K. R.; Baksi, A.; Ghosh, A.; Natarajan, G.; Som, A.; Pradeep, T. Interparticle Reactions: An Emerging Direction in Nanomaterials Chemistry. *Acc. Chem. Res.* **2017**, *50* (8), 1988–1996.
- (33) Krishnadas, K. R.; Baksi, A.; Ghosh, A.; Natarajan, G.; Pradeep, T. Manifestation of Geometric and Electronic Shell Structures of Metal Clusters in Intercluster Reactions. *ACS Nano* **2017**, *11* (6), 6015–6023.
- (34) Huang, B.; Pei, Y. On the mechanism of inter-cluster alloying reactions: two-stage metal exchange of [Au<sub>25</sub>(PET)<sub>18</sub>]<sup>−</sup> and [Ag<sub>25</sub>(DMBT)<sub>18</sub>]<sup>−</sup> clusters. *J. Mater. Chem. A* **2020**, *8* (20), 10242–10251.
- (35) Chakraborty, P.; Nag, A.; Natarajan, G.; Bandyopadhyay, N.; Paramasivam, G.; Panwar, M. K.; Chakrabarti, J.; Pradeep, T. Rapid isotopic exchange in nanoparticles. *Sci. Adv.* **2019**, *5* (1), eaau7555.
- (36) Neumaier, M.; Baksi, A.; Weis, P.; Schneider, E. K.; Chakraborty, P.; Hahn, H.; Pradeep, T.; Kappes, M. M. Kinetics of Intercluster Reactions between Atomically Precise Noble Metal Clusters [Ag<sub>25</sub>(DMBT)<sub>18</sub>]<sup>−</sup> and [Au<sub>25</sub>(PET)<sub>18</sub>]<sup>−</sup> in Room Temperature Solutions. *J. Am. Chem. Soc.* **2021**, *143* (18), 6969–6980.
- (37) Krishnadas, K. R.; Ghosh, A.; Baksi, A.; Chakraborty, I.; Natarajan, G.; Pradeep, T. Intercluster Reactions between Au<sub>25</sub>(SR)<sub>18</sub> and Ag<sub>44</sub>(SR)<sub>30</sub>. *J. Am. Chem. Soc.* **2016**, *138* (1), 140–148.
- (38) Krishnadas, K. R.; Baksi, A.; Ghosh, A.; Natarajan, G.; Pradeep, T. Structure-conserving spontaneous transformations between nanoparticles. *Nat. Commun.* **2016**, *7* (1), 13447.
- (39) Baksi, A.; Chakraborty, P.; Bhat, S.; Natarajan, G.; Pradeep, T. [Au<sub>25</sub>(SR)<sub>18</sub>]<sub>22</sub><sup>−</sup>: a noble metal cluster dimer in the gas phase. *Chem. Commun.* **2016**, *52* (54), 8397–8400.
- (40) Bodiuzzaman, M.; Nag, A.; Pradeep Narayanan, R.; Chakraborty, A.; Bag, R.; Paramasivam, G.; Natarajan, G.; Sekar, G.; Ghosh, S.; Pradeep, T. A covalently linked dimer of [Ag<sub>25</sub>(DMBT)<sub>18</sub>]<sup>−</sup>. *Chem. Commun.* **2019**, *55* (34), 5025–5028.
- (41) Sels, A.; Salassa, G.; Cousin, F.; Lee, L.-T.; Bürgi, T. Covalently bonded multimers of Au<sub>25</sub>(SBut)<sub>18</sub> as a conjugated system. *Nanoscale* **2018**, *10* (26), 12754–12762.
- (42) Lahtinen, T.; Hulkko, E.; Sokolowska, K.; Tero, T.-R.; Saarnio, V.; Lindgren, J.; Pettersson, M.; Häkkinen, H.; Lehtovaara, L. Covalently linked multimers of gold nanoclusters Au<sub>102</sub>(p-MBA)<sub>44</sub> and Au ~ 250(p-MBA)<sub>n</sub>. *Nanoscale* **2016**, *8* (44), 18665–18674.
- (43) Chakraborty, P.; Baksi, A.; Mudedla, S. K.; Nag, A.; Paramasivam, G.; Subramanian, V.; Pradeep, T. Understanding proton capture and cation-induced dimerization of [Ag<sub>29</sub>(BDT)<sub>12</sub>]<sub>3</sub><sup>−</sup> clusters by ion mobility mass spectrometry. *Phys. Chem. Chem. Phys.* **2018**, *20* (11), 7593–7603.
- (44) Kang, X.; Wang, S.; Zhu, M. Observation of a new type of aggregation-induced emission in nanoclusters. *Chem. Sci.* **2018**, *9* (11), 3062–3068.
- (45) Ghosh, A.; Mohammed, O. F.; Bakr, O. M. Atomic-Level Doping of Metal Clusters. *Acc. Chem. Res.* **2018**, *51* (12), 3094–3103.
- (46) Khatun, E.; Ghosh, A.; Chakraborty, P.; Singh, P.; Bodiuzzaman, M.; Ganesan, P.; Natarajan, G.; Ghosh, J.; Pal, S. K.; Pradeep, T. A thirty-fold photoluminescence enhancement induced by secondary ligands in monolayer protected silver clusters. *Nanoscale* **2018**, *10* (42), 20033–20042.
- (47) Zeng, C.; Chen, Y.; Kirschbaum, K.; Lambright, K. J.; Jin, R. Emergence of hierarchical structural complexities in nanoparticles and their assembly. *Science* **2016**, *354* (6319), 1580.
- (48) Yan, N.; Xia, N.; Liao, L.; Zhu, M.; Jin, F.; Jin, R.; Wu, Z. Unraveling the long-pursued Au<sub>144</sub> structure by x-ray crystallography. *Sci. Adv.* **2018**, *4* (10), eaat7259.
- (49) Zeng, C.; Chen, Y.; Kirschbaum, K.; Appavoo, K.; Sfeir, M. Y.; Jin, R. Structural patterns at all scales in a nonmetallic chiral Au<sub>133</sub>(SR)<sub>52</sub> nanoparticle. *Sci. Adv.* **2015**, *1* (2), e1500045.
- (50) Liao, L.; Chen, J.; Wang, C.; Zhuang, S.; Yan, N.; Yao, C.; Xia, N.; Li, L.; Bao, X.; Wu, Z. Transition-sized Au<sub>92</sub> nanoparticle bridging non-fcc-structured gold nanoclusters and fcc-structured gold nanocrystals. *Chem. Commun.* **2016**, *52* (81), 12036–12039.
- (51) Gan, Z.; Chen, J.; Liao, L.; Zhang, H.; Wu, Z. Surface Single-Atom Tailoring of a Gold Nanoparticle. *J. Phys. Chem. Lett.* **2018**, *9* (1), 204–208.
- (52) Liu, X.; Chen, J.; Yuan, J.; Li, Y.; Li, J.; Zhou, S.; Yao, C.; Liao, L.; Zhuang, S.; Zhao, Y.; Deng, H.; Yang, J.; Wu, Z. A Silver Nanocluster Containing Interstitial Sulfur and Unprecedented Chemical Bonds. *Angew. Chem., Int. Ed.* **2018**, *57* (35), 11273–11277.
- (53) Nag, A.; Chakraborty, P.; Bodiuzzaman, M.; Ahuja, T.; Antharjanam, S.; Pradeep, T. Polymorphism of Ag<sub>29</sub>(BDT)<sub>12</sub>(TPP)<sub>43</sub><sup>−</sup> cluster: interactions of secondary ligands and their effect on solid state luminescence. *Nanoscale* **2018**, *10* (21), 9851–9855.
- (54) Higaki, T.; Liu, C.; Zhou, M.; Luo, T.-Y.; Rosi, N. L.; Jin, R. Tailoring the Structure of 58-Electron Gold Nanoclusters: Au<sub>103</sub>S<sub>2</sub>(S-Nap)<sub>41</sub> and Its Implications. *J. Am. Chem. Soc.* **2017**, *139* (29), 9994–10001.
- (55) Khatun, E.; Bodiuzzaman, M.; Sugi, K. S.; Chakraborty, P.; Paramasivam, G.; Dar, W. A.; Ahuja, T.; Antharjanam, S.; Pradeep, T. Confining an Ag<sub>10</sub> Core in an Ag<sub>12</sub> Shell: A Four-Electron Superatom with Enhanced Photoluminescence upon Crystallization. *ACS Nano* **2019**, *13* (5), 5753–5759.
- (56) Hossain, S.; Imai, Y.; Motohashi, Y.; Chen, Z.; Suzuki, D.; Suzuki, T.; Kataoka, Y.; Hirata, M.; Ono, T.; Kurashige, W.; Kawawaki, T.; Yamamoto, T.; Negishi, Y. Understanding and designing one-dimensional assemblies of ligand-protected metal nanoclusters. *Mater. Horiz.* **2020**, *7* (3), 796–803.
- (57) Narouz, M. R.; Takano, S.; Lummis, P. A.; Levchenko, T. I.; Nazemi, A.; Kaappa, S.; Malola, S.; Yousefzaladeh, G.; Calhoun, L. A.; Stampelcoskie, K. G.; Häkkinen, H.; Tsukuda, T.; Crudden, C. M. Robust, Highly Luminescent Au<sub>13</sub> Superatoms Protected by N-Heterocyclic Carbenes. *J. Am. Chem. Soc.* **2019**, *141* (38), 14997–15002.
- (58) Wei, X.; Kang, X.; Yuan, Q.; Qin, C.; Jin, S.; Wang, S.; Zhu, M. Capture of Cesium Ions with Nanoclusters: Effects on Inter- and Intramolecular Assembly. *Chem. Mater.* **2019**, *31* (13), 4945–4952.
- (59) Kang, X.; Wei, X.; Xiang, P.; Tian, X.; Zuo, Z.; Song, F.; Wang, S.; Zhu, M. Rendering hydrophobic nanoclusters water-soluble and biocompatible. *Chem. Sci.* **2020**, *11* (18), 4808–4816.
- (60) Chang, H.; Karan, N. S.; Shin, K.; Bootharaju, M. S.; Nah, S.; Chae, S. I.; Baek, W.; Lee, S.; Kim, J.; Son, Y. J.; Kang, T.; Ko, G.; Kwon, S.-H.; Hyeon, T. Highly Fluorescent Gold Cluster Assembly. *J. Am. Chem. Soc.* **2021**, *143* (1), 326–334.
- (61) Li, Q.; Russell, J. C.; Luo, T.-Y.; Roy, X.; Rosi, N. L.; Zhu, Y.; Jin, R. Modulating the hierarchical fibrous assembly of Au nanoparticles with atomic precision. *Nat. Commun.* **2018**, *9* (1), 3871.
- (62) Udayabhaskarao, T.; Bootharaju, M. S.; Pradeep, T. Thiolate-protected Ag<sub>32</sub> clusters: mass spectral studies of composition and insights into the Ag–thiolate structure from NMR. *Nanoscale* **2013**, *5* (19), 9404–9411.
- (63) Som, A.; Samal, A. K.; Udayabhaskarao, T.; Bootharaju, M. S.; Pradeep, T. Manifestation of the Difference in Reactivity of Silver Clusters in Contrast to Its Ions and Nanoparticles: The Growth of Metal Tipped Te Nanowires. *Chem. Mater.* **2014**, *26* (10), 3049–3056.
- (64) Som, A.; Chakraborty, I.; Maark, T. A.; Bhat, S.; Pradeep, T. Cluster-Mediated Crossed Bilayer Precision Assemblies of 1D Nanowires. *Adv. Mater.* **2016**, *28* (14), 2827–2833.

- (65) Chakraborty, A.; Fernandez, A. C.; Som, A.; Mondal, B.; Natarajan, G.; Paramasivam, G.; Lahtinen, T.; Häkkinen, H.; Nonappa; Pradeep, T. Atomically Precise Nanocluster Assemblies Encapsulating Plasmonic Gold Nanorods. *Angew. Chem., Int. Ed.* **2018**, *57* (22), 6522–6526.
- (66) Bose, P.; Chakraborty, P.; Mohanty, J. S.; Nonappa; Ray; Chowdhuri, A.; Khatun, E.; Ahuja, T.; Mahendranath, A.; Pradeep, T. Atom transfer between precision nanoclusters and polydispersed nanoparticles: a facile route for monodisperse alloy nanoparticles and their superstructures. *Nanoscale* **2020**, *12* (43), 22116–22128.
- (67) Nonappa; Lahtinen, T.; Haataja, J. S.; Tero, T.-R.; Häkkinen, H.; Ikkala, O. Template-Free Supracolloidal Self-Assembly of Atomically Precise Gold Nanoclusters: From 2D Colloidal Crystals to Spherical Capsids. *Angew. Chem., Int. Ed.* **2016**, *55* (52), 16035–16038.
- (68) Nonappa; Ikkala, O. Hydrogen Bonding Directed Colloidal Self-Assembly of Nanoparticles into 2D Crystals, Capsids, and Supracolloidal Assemblies. *Adv. Funct. Mater.* **2018**, *28* (27), 1704328.
- (69) Chakraborty, P.; Nag, A.; Paramasivam, G.; Natarajan, G.; Pradeep, T. Fullerene-Functionalized Monolayer-Protected Silver Clusters: [Ag<sub>29</sub>(BDT)<sub>12</sub>(C60)<sub>n</sub>]<sub>3</sub>– (n = 1–9). *ACS Nano* **2018**, *12* (3), 2415–2425.
- (70) Chakraborty, P.; Nag, A.; Mondal, B.; Khatun, E.; Paramasivam, G.; Pradeep, T. Fullerene-Mediated Aggregation of M<sub>25</sub>(SR)<sub>18</sub>– (M = Ag, Au) Nanoclusters. *J. Phys. Chem. C* **2020**, *124* (27), 14891–14900.
- (71) Schulz-Dobrick, M.; Jansen, M. Intercluster Compounds Consisting of Gold Clusters and Fullerenes: [Au<sub>7</sub>(PPh<sub>3</sub>)<sub>7</sub>]<sub>2</sub>C<sub>60</sub>-THF and [Au<sub>8</sub>(PPh<sub>3</sub>)<sub>8</sub>]<sub>2</sub>(C<sub>60</sub>)<sub>2</sub>. *Angew. Chem., Int. Ed.* **2008**, *47* (12), 2256–2259.
- (72) Mathew, A.; Natarajan, G.; Lehtovaara, L.; Häkkinen, H.; Kumar, R. M.; Subramanian, V.; Jaleel, A.; Pradeep, T. Supramolecular Functionalization and Concomitant Enhancement in Properties of Au<sub>25</sub> Clusters. *ACS Nano* **2014**, *8* (1), 139–152.
- (73) Yan, C.; Liu, C.; Abroshan, H.; Li, Z.; Qiu, R.; Li, G. Surface modification of adamantane-terminated gold nanoclusters using cyclodextrins. *Phys. Chem. Chem. Phys.* **2016**, *18* (33), 23358–23364.
- (74) Bhunia, S.; Kumar, S.; Purkayastha, P. Gold Nanocluster-Grafted Cyclodextrin Suprastructures: Formation of Nanospheres to Nanocubes with Intriguing Photophysics. *ACS Omega* **2018**, *3* (2), 1492–1497.
- (75) Chen, Y.; Liu, C.; Tang, Q.; Zeng, C.; Higaki, T.; Das, A.; Jiang, D.-e.; Rosi, N. L.; Jin, R. Isomerism in Au<sub>28</sub>(SR)<sub>20</sub> Nanocluster and Stable Structures. *J. Am. Chem. Soc.* **2016**, *138* (5), 1482–1485.
- (76) Kang, X.; Zhu, M. Structural Isomerism in Atomically Precise Nanoclusters. *Chem. Mater.* **2021**, *33* (1), 39–62.
- (77) Xu, W. W.; Zeng, X. C.; Gao, Y. The structural isomerism in gold nanoclusters. *Nanoscale* **2018**, *10* (20), 9476–9483.
- (78) Matus, M. F.; Malola, S.; Kinder Bonilla, E.; Barngrover, B. M.; Aikens, C. M.; Häkkinen, H. A topological isomer of the Au<sub>25</sub>(SR)<sub>18</sub>– nanocluster. *Chem. Commun.* **2020**, *56* (58), 8087–8090.
- (79) Qin, Z.; Zhang, J.; Wan, C.; Liu, S.; Abroshan, H.; Jin, R.; Li, G. Atomically precise nanoclusters with reversible isomeric transformation for rotary nanomotors. *Nat. Commun.* **2020**, *11* (1), 6019.
- (80) Baksi, A.; Ghosh, A.; Mudedla, S. K.; Chakraborty, P.; Bhat, S.; Mondal, B.; Krishnadas, K. R.; Subramanian, V.; Pradeep, T. Isomerism in Monolayer Protected Silver Cluster Ions: An Ion Mobility-Mass Spectrometry Approach. *J. Phys. Chem. C* **2017**, *121* (24), 13421–13427.
- (81) Nag, A.; Chakraborty, P.; Paramasivam, G.; Bodiuzzaman, M.; Natarajan, G.; Pradeep, T. Isomerism in Supramolecular Adducts of Atomically Precise Nanoparticles. *J. Am. Chem. Soc.* **2018**, *140* (42), 13590–13593.
- (82) Jiang, T.; Qu, G.; Wang, J.; Ma, X.; Tian, H. Cucurbiturils brighten Au nanoclusters in water. *Chem. Sci.* **2020**, *11* (13), 3531–3537.
- (83) van der Linden, M.; Barendregt, A.; van Bunningen, A. J.; Chin, P. T. K.; Thies-Weesie, D.; de Groot, F. M. F.; Meijerink, A. Characterisation, degradation and regeneration of luminescent Ag<sub>29</sub> clusters in solution. *Nanoscale* **2016**, *8* (47), 19901–19909.
- (84) Black, D. M.; Robles, G.; Lopez, P.; Bach, S. B. H.; Alvarez, M.; Whetten, R. L. Liquid Chromatography Separation and Mass Spectrometry Detection of Silver-Lipoate Ag<sub>29</sub>(LA)<sub>12</sub> Nanoclusters: Evidence of Isomerism in the Solution Phase. *Anal. Chem.* **2018**, *90* (3), 2010–2017.
- (85) Nag, A.; Chakraborty, P.; Thacharon, A.; Paramasivam, G.; Mondal, B.; Bodiuzzaman, M.; Pradeep, T. Atomically Precise Noble Metal Cluster-Assembled Superstructures in Water: Luminescence Enhancement and Sensing. *J. Phys. Chem. C* **2020**, *124* (40), 22298–22303.
- (86) Chakraborty, P.; Nag, A.; Sugi, K. S.; Ahuja, T.; Varghese, B.; Pradeep, T. Crystallization of a Supramolecular Coassembly of an Atomically Precise Nanoparticle with a Crown Ether. *ACS Mater. Lett.* **2019**, *1* (5), 534–540.
- (87) Muhammed, M. A. H.; Cruz, L. K.; Emwas, A.-H.; El-Zohry, A. M.; Moosa, B.; Mohammed, O. F.; Khashab, N. M. Pillar[5]arene-Stabilized Silver Nanoclusters: Extraordinary Stability and Luminescence Enhancement Induced by Host–Guest Interactions. *Angew. Chem., Int. Ed.* **2019**, *58* (44), 15665–15670.
- (88) Bootharaju, M. S.; Dey, R.; Gevers, L. E.; Hedhili, M. N.; Basset, J.-M.; Bakr, O. M. A New Class of Atomically Precise, Hydride-Rich Silver Nanoclusters Co-Protected by Phosphines. *J. Am. Chem. Soc.* **2016**, *138* (42), 13770–13773.
- (89) Almansaf, A. A.; Parida, M. R.; Besong, T. M. D.; Maity, P.; Bootharaju, M. S.; Bakr, O. M.; Mohammed, O. F. The impact of Au doping on the charge carrier dynamics at the interfaces between cationic porphyrin and silver nanoclusters. *Chem. Phys. Lett.* **2017**, *683*, 393–397.
- (90) Sugi, K. S.; Bandyopadhyay, P.; Bodiuzzaman, M.; Nag, A.; Hridya, M.; Dar, W. A.; Ghosh, P.; Pradeep, T. Manifestation of Structural Differences of Atomically Precise Cluster-Assembled Solids in Their Mechanical Properties. *Chem. Mater.* **2020**, *32* (18), 7973–7984.
- (91) Roy, X.; Lee, C.-H.; Crowther, A. C.; Schenck, C. L.; Besara, T.; Lalancette, R. A.; Siegrist, T.; Stephens, P. W.; Brus, L. E.; Kim, P.; Steigerwald, M. L.; Nuckolls, C. Nanoscale Atoms in Solid-State Chemistry. *Science* **2013**, *341* (6142), 157.
- (92) Fetzer, F.; Maier, A.; Hodas, M.; Geladari, O.; Braun, K.; Meixner, A. J.; Schreiber, F.; Schnepf, A.; Scheele, M. Structural order enhances charge carrier transport in self-assembled Au-nanoclusters. *Nat. Commun.* **2020**, *11* (1), 6188.
- (93) Wang, Y.-M.; Zhang, J.-W.; Wang, Q.-Y.; Li, H.-Y.; Dong, X.-Y.; Wang, S.; Zang, S.-Q. Fabrication of silver chalcogenolate cluster hybrid membranes with enhanced structural stability and luminescence efficiency. *Chem. Commun.* **2019**, *55* (97), 14677–14680.
- (94) Basu, S.; Hajra, A.; Gayen, C.; Paul, A. Zinc-Ion-Induced Aggregation of Gold Clusters for Visible-Light-Excitation-Based Fluorimetric Discrimination of Geometrical Isomers. *ChemPhysChem* **2020**, *21* (8), 809–813.
- (95) Yang, Y.; Wang, S.; Zhou, Y.; Wang, X.; Liu, X.; Xie, A.; Shen, Y.; Zhu, M. Structurally accurate lipophilic Pt<sub>1</sub>Ag<sub>28</sub> nanoclusters based cancer theranostic micelles for dual-targeting/aggregation enhanced fluorescence imaging and photothermal/photodynamic therapies. *Colloids Surf., B* **2020**, *196*, 111346.
- (96) Zhang, C.; Zhang, A.; Hou, W.; Li, T.; Wang, K.; Zhang, Q.; de la Fuente, J. M.; Jin, W.; Cui, D. Mimicking Pathogenic Invasion with the Complexes of Au<sub>22</sub>(SG)<sub>18</sub>-Engineered Assemblies and Folic Acid. *ACS Nano* **2018**, *12* (5), 4408–4418.
- (97) Zhu, H.; Goswami, N.; Yao, Q.; Chen, T.; Liu, Y.; Xu, Q.; Chen, D.; Lu, J.; Xie, J. Cyclodextrin–gold nanocluster decorated TiO<sub>2</sub> enhances photocatalytic decomposition of organic pollutants. *J. Mater. Chem. A* **2018**, *6* (3), 1102–1108.
- (98) Zhao, Y.; Zhuang, S.; Liao, L.; Wang, C.; Xia, N.; Gan, Z.; Gu, W.; Li, J.; Deng, H.; Wu, Z. A Dual Purpose Strategy to Endow Gold Nanoclusters with Both Catalysis Activity and Water Solubility. *J. Am. Chem. Soc.* **2020**, *142* (2), 973–977.

(99) Wu, Z.; Liu, J.; Gao, Y.; Liu, H.; Li, T.; Zou, H.; Wang, Z.; Zhang, K.; Wang, Y.; Zhang, H.; Yang, B. Assembly-Induced Enhancement of Cu Nanoclusters Luminescence with Mechanochromic Property. *J. Am. Chem. Soc.* **2015**, *137* (40), 12906–12913.

(100) Huang, H.-Y.; Cai, K.-B.; Talite, M. J.; Chou, W.-C.; Chen, P.-W.; Yuan, C.-T. Coordination-induced emission enhancement in gold-nanoclusters with solid-state quantum yields up to 40% for eco-friendly, low-reabsorption nano-phosphors. *Sci. Rep.* **2019**, *9* (1), 4053.

(101) Moussawi, M. A.; Leclerc-Laronze, N.; Floquet, S.; Abramov, P. A.; Sokolov, M. N.; Cordier, S.; Ponchel, A.; Monflier, E.; Bricout, H.; Landy, D.; Haouas, M.; Marrot, J.; Cadot, E. Polyoxometalate, Cationic Cluster, and  $\gamma$ -Cyclodextrin: From Primary Interactions to Supramolecular Hybrid Materials. *J. Am. Chem. Soc.* **2017**, *139* (36), 12793–12803.

(102) Ong, W.-L.; O'Brien, E. S.; Dougherty, P. S. M.; Paley, D. W.; Fred Higgs, C., III; McGaughey, A. J. H.; Malen, J. A.; Roy, X. Orientational order controls crystalline and amorphous thermal transport in superatomic crystals. *Nat. Mater.* **2017**, *16* (1), 83–88.

(103) Pinkard, A.; Champsaur, A. M.; Roy, X. Molecular Clusters: Nanoscale Building Blocks for Solid-State Materials. *Acc. Chem. Res.* **2018**, *51* (4), 919–929.